

Density-Softmax: Scalable and Calibrated Uncertainty Estimation under Distribution Shifts

Ha Manh Bui¹ Anqi Liu¹

¹ Department of Computer Science, Johns Hopkins University, Baltimore, Maryland, USA *

Abstract

Prevalent deterministic deep-learning models suffer from significant over-confidence under distribution shifts. Probabilistic approaches can reduce this problem but struggle with computational efficiency. In this paper, we propose Density-Softmax, a fast and lightweight deterministic method to improve calibrated uncertainty estimation via a combination of density function with the softmax layer. By using the latent representation’s likelihood value, our approach produces more uncertain predictions when test samples are distant from the training samples. Theoretically, we show that Density-Softmax can produce high-quality uncertainty estimation with neural networks, as it is the solution of minimax uncertainty risk and is distance-aware, thus reducing the over-confidence of the standard softmax. Empirically, our method enjoys similar computational efficiency as a single forward pass deterministic with standard softmax on the shifted toy, vision, and language datasets across modern deep-learning architectures. Notably, Density-Softmax uses 4 times fewer parameters than Deep Ensembles and 6 times lower latency than Rank-1 Bayesian Neural Network, while obtaining competitive predictive performance and lower calibration errors under distribution shifts.

1 Introduction

The ability to produce calibrated uncertainty estimates is crucial for deploying DNN solutions in high-stake applications such as healthcare and autonomous driving [1–3]. However, common DNN nowadays which rely on the softmax layer to produce predictive distribution are poorly calibrated and over-confident [4, 5]. This poor performance often occurs in real-world applications under distribution shifts, where training data does not come from the same distribution as the test data [6–8].

To achieve calibrated uncertainty and robustness, recent Probabilistic Modelling techniques including Gaussian Process [9–11], Dropout [12–14], and BNN [15–18] have shown promising results. Among these works, the best performance in practice so far is based on Deep Ensembles [5, 19, 20]. However, compared with a single deterministic DNN [21], which only needs a single forward pass to produce softmax uncertainty, the aforementioned probabilistic approaches suffer from a heavy computational burden due to often needing more parameters and multiple forward passes in inference. For example, one inference step for Rank-1 BNN [18] can take 6 times longer than a single deterministic DNN or Deep Ensembles often more than 4 times in terms of the number of parameters. As a consequence, these probabilistic models become unscalable in real-world applications.

Toward scalability and high-quality uncertainty estimation, novel deterministic-based methods have been proposed recently [11, 22–26]. Nevertheless, these works often only focus on improving uncertainty estimation in terms of binary OOD detection. Meanwhile, the over-under-confidence with multi-class issues under distribution shifts, which belong to calibrated uncertainty, has not been focused on [22, 24–26]. As a result, the aforementioned approaches either are not able to measure calibration by there is no multi-class classification layer [25–27], fail in calibration performance [5, 22, 24, 28], or require re-calibration steps [4, 23, 28–30]. Recently, SNGP [11] has shown promising results in both OOD detection and calibration under distribution

*Correspondence to Ha Manh Bui: <hb.buimanhha@gmail.com>.

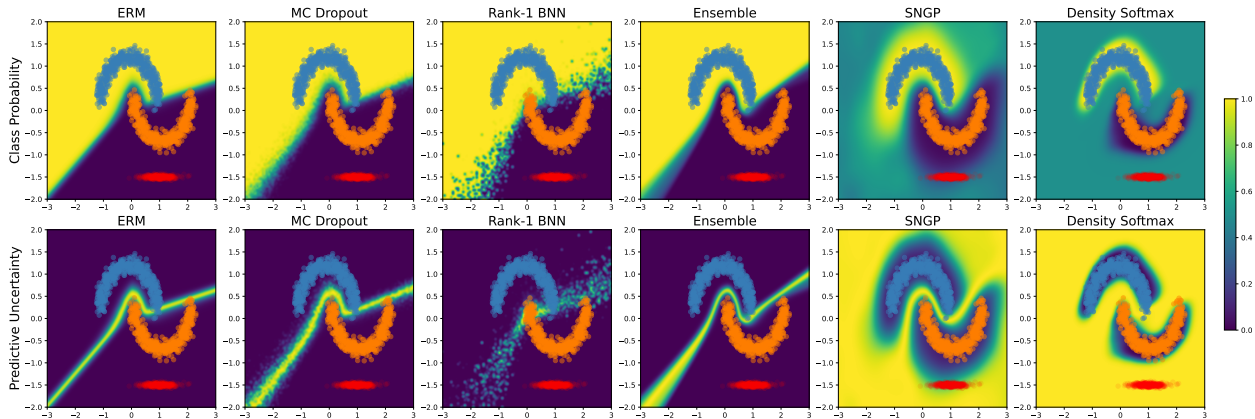


Figure 1: The class probability $p(y|x)$ (Top Row) and predictive uncertainty $var(y|x) = p(y|x) * (1 - p(y|x))$ surface (Bottom Row) of our Density-Softmax v.s. different approaches on the two moons 2D classification. Training data for positive (Orange) and negative classes (Blue). OOD data (Red) are not observed during training. Background color represents the estimated model’s class probability and predictive uncertainty. **Our Density-Softmax achieves distance awareness with a uniform class probability and high uncertainty value on OOD data.** The detail of this dataset is in Appendix C.1. The detail of this experiment is in Section 6.2. *A quick demo is available at https://colab.research.google.com/drive/1zU13WPQRfZzfW609f0OxseSkhZiGTw5N?usp=share_link.*

shifts by using a distance-aware model. Yet, its computational requirements are still higher than a single deterministic model across modern DNN architectures due to their additional non-trainable parameters with the power iteration method [31], and MC sampling in practice (e.g., it needs a two times higher number of parameters¹ with Resnet-50 while two times longer latency with Wide Resnet-28-10 in Figure 4).

Toward a model with the same computational efficiency as a single deterministic DNN, we propose Density-Softmax which is motivated by the idea of using distance awareness to improve the uncertainty quality under distribution shifts. Our model includes 4 main components: a feature extractor, a statistical density model on latent (feature) space, a classifier, and a softmax layer. The key component is the density function, by using its likelihood value as an in-out-distribution detector, we can combine it with the softmax layer to improve the predictive uncertainty. The weight of the classifier is then re-optimized with the likelihood value to enhance robust generalization.

Our contributions can be summarized as:

1. We introduce Density-Softmax, a reliable, fast, and lightweight DNN framework via a direct combination of density function with the softmax layer. Notably, our algorithm does not require any OOD set or the re-calibration technique in training.
2. We formally prove that our method produces a uniform prediction for OOD and confident in-domain prediction for IID data. Furthermore, we prove the solution of the minimax uncertainty risk, distance awareness, and reducing over-confidence of the standard softmax of our procedure assuming that we can estimate densities in low dimensions.
3. We empirically show our framework achieves distance awareness while having competitive uncertainty estimation performance in both calibration and OOD detection with probabilistic models on the Toy, shifted CIFAR-10, CIFAR-100, ImageNet with ResNet, and CLINC OOS language with BERT. More importantly, Density-Softmax requires only a single forward pass, therefore has fewer parameters and is much faster than other baselines at the inference step.

2 Related Work

Uncertainty and Robustness via Probabilistic Modeling. More modern discussion of Reliable Machine Learning can be found in the literature on Reliability Baselines [7]. For the uncertainty and robustness under distributional shifts [8], Nado et al. [5] has studied extensively in the benchmark for a fair comparison between SOTA methods, mainly evaluating NLL, in-out accuracy for generalization, and ECE for calibrated uncertainty. Probabilistic Modeling is a widely used approach for improving the reliability of DNN [5, 7]. Starting with Gaussian Process [9–11], Dropout [12–14], and the SOTA Ensembles [19, 20, 32]. Then with BNN [16] and its multiple variants, including Laplace [17], SGLD [33], SWAG [34], MFVI [15], and Rank-1 BNN [18].

Deterministic Uncertainty. *The Probabilistic Models, however, are limited in scalability.* To tackle this challenge, novel deterministic-based methods have been investigated, including replacing the loss

function [25, 28, 35–39], the output layer [22, 23, 26, 40–42], or computing a closed-form posterior by conjugate prior in Bayesian inference [24, 43–47]. Nevertheless, many of these works still have limitations, including requiring access to OOD samples during training time [35, 36, 48], being designed only for binary or regression tasks [26, 27, 29, 45], and requiring re-calibration techniques [23, 28–30, 39, 40]. OOD detection is a downstream task of uncertainty estimation [4–7, 27]. Popular approaches in this direction often only aim to improve AUPR/AUROC and treat the OOD detection as a binary problem in parallel with the class prediction, i.e., their OOD detector often predicts variance value independently with the class probability [23, 27, 38, 40]. As a consequence, such methods are not explicitly designed to improve calibrated uncertainty and do not evaluate calibration [25, 26, 37, 41, 42]. Especially, in some OOD detection methods [25–27], there is no multi-classification layer to measure calibration. *In contrast, our method uses the probability of softmax directly for computing the variance, which can benefit both calibration and OOD detection.*

In the scope of multi-class classification and calibration setting [5, 7], closest to our work is DUQ [22] and SNGP [11]. Although DUQ can reduce latency by using kernel distance, it still has high storage demands as well as a significantly lower uncertainty and robustness quality than SOTA [5, 11]. SNGP then can improve these performances by using a distance-aware model. However, it also suffers from the model size and latency because requiring non-trainable parameters to do Spectral Normalization for every weight in each residual layer with the power iteration method [31, 49]. Additionally, although SNGP theoretically can use mean-field, it empirically still uses MC sampling to boost model performance, increasing latency with multiple forward passes. *Our method is thus a light-weighted reliable DNN method that is computational and storage efficient by using only a single forward pass.*

Uncertainty via Density Estimation. Improving uncertainty via Density Estimation has recently been investigated [23, 24, 30, 38, 40]. However, Kuleshov and Deshpande [30]’s work needs re-calibration steps and estimate density on label space by the re-calibrator. Regarding deterministic approaches, Posterior Net [24] estimates multiple conditional densities per class and needs to select a good Prior distribution with additional hyper-parameters for tuning Bayesian loss, which is often difficult in practice [7, 44, 45, 47]. Meanwhile, although DDU [23, 40] and NUQ [38] also use the density function to detect OOD, these OOD detectors do not contribute to the predictive distribution directly, causing uncalibrated prediction (see Figure 4). Consequently, DDU evaluates calibration only after applying the post-hoc re-calibration technique. Additionally, NUQ is based on a non-parametric model with KNN, therefore, unscalable when the number of training data points increases. *In contrast, our method is a parametric model and does not include any re-calibration step.*

3 Background

3.1 Distributional Shifts

Notation and Problem setting. Let $\mathcal{X} \subset \mathbb{R}^{d_x}$ be the sample space and $\mathcal{Y} \subset \mathbb{R}$ be the label space. Denote the set of joint probability distributions on $\mathcal{X} \times \mathcal{Y}$ by $\mathcal{P}_{\mathcal{X} \times \mathcal{Y}}$. A dataset is defined by a joint distribution $\mathbb{P}(x, y) \in \mathcal{P}_{\mathcal{X} \times \mathcal{Y}}$, and let \mathcal{P} be a measure on $\mathcal{P}_{\mathcal{X} \times \mathcal{Y}}$, i.e., whose realizations are distributions on $\mathcal{X} \times \mathcal{Y}$. Denote training data by $D_s = \{(x_i, y_i)\}_{i=1}^n$, where n is the number of data points in D_s , i.e., $(x_i, y_i) \sim \mathbb{P}_s(x, y)$ and $\mathbb{P}_s(x, y) \sim \mathcal{P}$. In a standard machine learning setting, a learning model which is only trained on the training data D_s , arrives at a good generalization performance on the test dataset $D_t = \{(x_j, y_j)\}_{j=1}^m$, where m is the number of data points in D_t , i.e., $(x_j, y_j) \sim \mathbb{P}_t(x, y)$ and $\mathbb{P}_t(x, y) \sim \mathcal{P}$. In the typical Independent-identically-distributed (IID) setting, the joint distribution between $\mathbb{P}_t(x, y)$ is similar to $\mathbb{P}_s(x, y)$, and let us use $\mathbb{P}_{iid}(x, y)$ to represent the IID test distribution. In contrast, $\mathbb{P}_t(x, y)$ is different with $\mathbb{P}_s(x, y)$ if D_t is Out-of-Distribution (OOD) data, and let us use $\mathbb{P}_{ood}(x, y)$ to represent the OOD test distribution.

In OOD setting, we consider two types of shifts—**covariate shift** and **semantic shift** [6, 7]. Formally, covariate shift means that OOD samples $x_{ood} \sim \mathbb{P}_{ood}(x)$ and $y_{ood} \sim \mathbb{P}_{iid}(y|x)$. For example, a model is trained on CIFAR-10 and tested on OOD samples with some noise on the test image of CIFAR-10-C. We use this covariate shift setting to evaluate the uncertainty and robustness of methods. Meanwhile, the semantic shift means that $(x_{ood}, y_{ood}) \sim \mathbb{P}_{ood}(x, y)$ and $\mathcal{Y}_{iid} \neq \mathcal{Y}_{ood}$. For instance, a model is trained on CIFAR-10 and tested on CIFAR-100 OOD samples. We use semantic shift as an extreme case to evaluate distance awareness because every prediction will be misclassified in this setting and the model should always be uncertain about its prediction.

3.2 Calibrated Classification

In the classification setting of representation learning, we predict a target $y \in \mathcal{Y}$, where \mathcal{Y} is discrete with K possible categories by using a forecast $h = \sigma(g \circ f)$, which composites a feature extractor $f : \mathcal{X} \rightarrow \mathcal{Z}$, where $\mathcal{Z} \subset \mathbb{R}^{d_z}$ is latent space, a classifier embedding $g : \mathcal{Z} \rightarrow \mathbb{R}^K$, and a softmax layer $\sigma : \mathbb{R}^K \rightarrow \Delta_{\mathcal{Y}}$ which outputs a probability distribution $W(y) : \mathcal{Y} \rightarrow [0, 1]$ within the set $\Delta_{\mathcal{Y}}$ of distributions over \mathcal{Y} ; the probability density function of W is w . First, we present the definition of distribution calibration for the forecast:

Definition 3.1. [50, 51] A forecast h is said to be **distributional calibrated** if

$$\mathbb{P}(Y = y \mid h(x) = W) = w(y), \forall y \in \mathcal{Y}, W \in \Delta_{\mathcal{Y}}. \quad (1)$$

Intuitively, this means the forecast h is well-calibrated if its outputs truthfully quantify the predictive uncertainty. For example, if we take all data points x for which the model predicts $[h(x)]_y = 0.3$, we expect 30% of them to indeed take on the label y . To quantify distributional calibrated in Definition 3.1, an approximate estimator of the Calibration Error [52] in expectation was given by Naeini et al. [53] and is still the most commonly used measure for a multi-class model. It is referred to as the **Expected Calibration Error (ECE)** of model $h : \mathcal{X} \rightarrow \Delta_{\mathcal{Y}}$ is defined as

$$\text{ECE}(h) := \sum_{m=1}^M \frac{|B_m|}{N} |\text{acc}(B_m) - \text{conf}(B_m)|, \quad (2)$$

where B_m is the set of sample indices whose confidence falls into $(\frac{m-1}{M}, \frac{m}{M}]$ in M bins, N is the number of samples, bin-wise mean accuracy $\text{acc}(B_m) := \frac{1}{|B_m|} \sum_{i \in B_m} \mathbb{I}(\arg \max_{y \in \mathcal{Y}} [h(x_i)]_y = y_i)$, and bin-wise mean confidence $\text{conf}(B_m) := \frac{1}{|B_m|} \sum_{i \in B_m} \max_{y \in \mathcal{Y}} [h(x_i)]_y$.

3.3 Distance Awareness

Although ECE is a popular metric to quantify the quality of predictive uncertainty, it has many known issues [54] such as it is sensitive to the number of bins [55]. Distance awareness, on the other hand, is important for evaluating uncertainty under distributional shifts since the sample distribution may vary like the OOD data in Figure 1 [22, 56–58]. Therefore, the definition of distance-aware uncertainty was introduced by Liu et al. [11] and defined as:

Definition 3.2. [11] Consider the predictive distribution of the softmax layer $\sigma(g(f(x_t)))$ on new test sample x_t , $\sigma(g(f(x_t)))$ is said to be **distance aware** if there exists $u(x_t)$, a summary statistics of $\sigma(g(f(x_t)))$, that quantifies model uncertainty (e.g., entropy, predictive variance, etc.) and reflects the distance between x_t and the training data X_s w.r.t. a metric $\|\cdot\|$, i.e.,

$$u(x_t) := v(d(x_t, X_s)), \quad (3)$$

where v is a monotonic function and $d(x_t, X_s) := \mathbb{E} \|x_t - X_s\|_{\mathcal{X}}$ is the distance between x_t and the training data X_s .

Following Definition 3.2, Liu et al. [11] provided two conditions for the logits $g \circ f$ of the forecast h to be distance aware. First, make the output of g distance aware so that it outputs an uncertainty metric reflecting distance in the latent space $\|f(x) - f(x')\|_{\mathcal{Z}}$. Second, making the feature extractor f distance preserving so that the distance in the latent space $\|f(x) - f(x')\|_{\mathcal{Z}}$ has a meaningful correspondence to the distance $\|x - x'\|_{\mathcal{X}}$ in the data manifold. *If a model achieves this distance aware property, then it can reduce over-confidence issues of current DNN on OOD while still can preserve certainty predictions for the IID test example, suggesting calibration improvement.*

3.4 Reliability v.s. Scalability

In order to create a robust model that achieves both calibration and distance-aware uncertainty, current approaches have focused on probabilistic modeling and ensembling [5, 7]. However, these methods are

struggling with scalability in real-world applications for two reasons. First, their number of parameters is often much higher than a single deterministic model, causing heavy memory storage requirements for ubiquitous hardware. Second, these models often need MC sampling during inference time, leading to a high latency cost in real-time applications. *Therefore, how to improve reliability while at the same time keeping the same computational requirements as a single deterministic model is still an open question to research.*

4 Density-Softmax

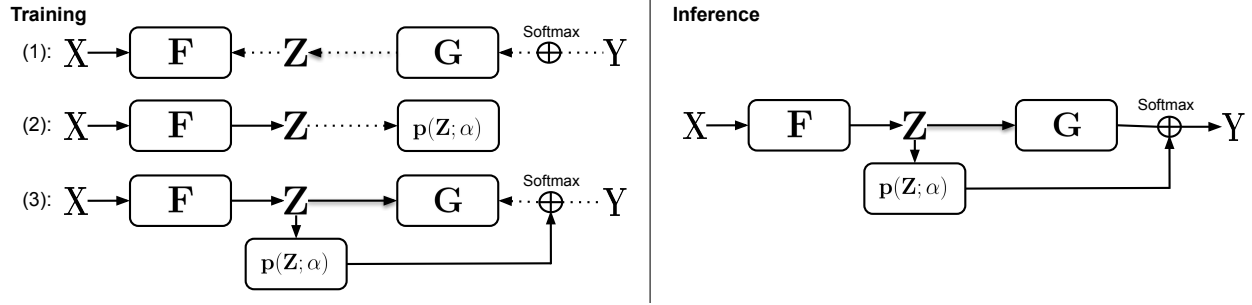


Figure 2: The overall architectures of Density-Softmax, including encoder f , classifier g , and density function $p(Z; \alpha)$. The rectangle boxes represent these functions. The dashed lines represent the backward, solid lines represent the forward pass. The circle with two cross lines represents the softmax layer. The 3 training steps and inference process follow Algorithm 1.

Toward a distance-aware and scalable framework, we propose Density-Softmax. Our idea is based on the solution of the **minimax uncertainty risk** [11, 59] as follows

$$\inf_{\mathbb{P}(Y|X) \in \mathcal{P}} \left[\sup_{\mathbb{P}^*(Y|X) \in \mathcal{P}^*} S(\mathbb{P}(Y|X), \mathbb{P}^*(Y|X)) \right], \quad (4)$$

where $S(\cdot, \mathbb{P}^*(Y|X))$ is strictly proper scoring rules [60, 61], $\mathbb{P}(Y|X)$ is predictive, and $\mathbb{P}^*(Y|X)$ is the data-generation distribution. Under the classification task and for the Brier Score [62], the solution of Equation 4 was shown by Liu et al. [11] as

$$\mathbb{P}(Y|X) = \mathbb{P}(Y|X_{iid})\mathbb{P}^*(X_{iid}) + \mathbb{U}(Y|X_{ood})\mathbb{P}^*(X_{ood}), \quad (5)$$

where X_{iid} is IID, X_{ood} is OOD sample variable, and \mathbb{U} stands for uniform distribution [59, 63]. According to Equation 5, we summarize the overview of Density-Softmax in Figure 2. Under our framework, the predictive distribution is equivalent to

$$\mathbb{P}(Y|X) = \sigma(p(Z; \alpha) * g(Z)), \text{ with } Z = f(X), \quad (6)$$

where $f: \mathcal{X} \rightarrow \mathcal{Z}$ is the feature extractor, $g: \mathcal{Z} \rightarrow \mathbb{R}^K$ is the last classifier layer, $\sigma: \mathbb{R}^K \rightarrow \Delta_y$ is the softmax layer, and $p(Z; \alpha)$ is the density function to measure the representation distance on latent space \mathcal{Z} .

Training. In the first training step, we optimize the model as normal by using ERM [21] from training data D_s by solving

$$\min_{\theta_{g,f}} \left\{ \mathbb{E}_{(x,y) \sim D_s} [-y \log(\sigma(g(f(x))))] \right\}, \quad (7)$$

where $\theta_{g,f}$ is the parameter of encoder f and classifier g .

After that, we fix the parameter θ_f of f to estimate density on representation space \mathcal{Z} by positing a statistical model for $p(Z; \alpha)$, then fitting MLE to yield $\hat{\alpha}$ and scale $p(Z; \hat{\alpha})$ to a specified range. The statistical density model $p(Z; \alpha)$ is varied across the dataset. In particular, for the toy dataset, we use KDE [64] since the dimension of latent space \mathcal{Z} is only 128. For the higher dimensions between 640 and 2048, we estimate the density by using Normalizing-Flows Real-NVP [65, 66] since it is simple and provides exact log-likelihood, defined by

$$\log(p(z; \alpha)) = \log(p(t; \alpha)) + \log \left| \det \left(\frac{\partial t}{\partial z} \right) \right|, \quad (8)$$

where random variable $t = s_\alpha(z)$ and s is a bijective differentiable function.

To enhance generalization after combining with the likelihood value of the density function $p(Z; \hat{\alpha})$, we re-update the weight of classifier g to normalize with the likelihood value by optimizing with the objective function as follows

$$\min_{\theta_g} \left\{ \mathbb{E}_{(x,y) \sim D_s} [-y \log(\sigma(p(z; \hat{\alpha}) * g(z)))] \right\}, \text{ where } z = f(x). \quad (9)$$

Inference. After completing the training process, for a new test x_t at the Inference step, we perform prediction by combining the density function on latent space $p(z_t; \hat{\alpha})$ and classifier g which are trained in the training step to make prediction by the following formula

$$p(y = i | x_t) = \frac{\exp(p(z_t; \hat{\alpha}) * (z_t^\top \theta_{g_i}))}{\sum_{j=1}^K \exp(p(z_t; \hat{\alpha}) * (z_t^\top \theta_{g_j}))}, \forall i \in \mathcal{Y}, \quad (10)$$

where $z_t = f(x_t)$ is the latent presentation for test sample x_t . The pseudo-code for the training and inference processes of our proposed Density-Softmax framework is presented in Algorithm 1. It is worth noticing that due to the likelihood $p(Z; \hat{\alpha}) \in (-\infty; +\infty)$, the exponential function in Equation 10 can return a *NaN* if the likelihood $p(Z; \hat{\alpha}) \rightarrow \infty$ in implementation. Therefore, we need to scale it to the range of $(0, 1]$ to avoid this numerical issue. The detail for controlling the scale of likelihood is provided in Appendix B.1.

Equation 10 suggests two intuitions. First, if x_t is OOD data, the distance between x_t and training data D_s should be high by a low likelihood value of $p(z_t; \hat{\alpha})$, then the prediction will go to uniform.

Second, if x_t is IID data, the distance between x_t and training data D_s should be small by a high likelihood value of $p(z_t; \hat{\alpha})$, then the prediction follows the in-domain predictive distribution. These two intuitions imply Density-Softmax can provide distance awareness as well as avoid over-confidence on OOD and under-confidence on IID test samples, showing calibration ability. In the next section, we will formally explain these properties.

5 Theoretical Analysis

Since estimating density on high-dimensional data such as images with millions of pixels is non-trivial [24, 30, 66, 67]. Our paper instead estimates in latent space which often only up to 2048 dimensions, therefore, it is reasonable to estimate the exact density function on latent space. We first formally assume an exact density function by:

Assumption 5.1. (Latent-Density). Consider the density function $p(Z; \alpha)$, where the likelihood value is scaled in range $(0; 1]$ on latent space \mathcal{Z} . Assume we can learn a good $p(Z; \alpha)$ such that for an IID test sample x_{iid} , we have a high likelihood value $p(z_{iid} = f(x_{iid}); \alpha) \rightarrow 1$ and low value $p(z_{ood} = f(x_{ood}); \alpha) \rightarrow 0$ with OOD test sample x_{ood} .

This assumption is reasonable and is empirically shown in Figure 6 with high likelihood values on the CIFAR-10 IID test set and low values on the CIFAR-10-C OOD set. Following Assumption 5.1, we first show our framework can solve the non-uniform prediction of OOD data by providing a uniform predictive distribution in the following theorem:

Theorem 5.2. (Uniform prediction for OOD data). Consider x_{ood} and assume the out-domain prediction of the softmax layer with the model which has already been learned from training data is non-uniform: $\sigma(g(f(x_{ood}))) \neq \mathbb{U}$. Density-Softmax provides a uniform prediction for x_{ood} by multiplication with a low likelihood value $p(z_{ood} = f(x_{ood}); \alpha) \rightarrow 0$, i.e.,

$$\sigma(p(z_{ood}; \alpha) * g(z_{ood})) = \mathbb{U}, \text{ where } z_{ood} = f(x_{ood}).$$

Algorithm 1 Density-Softmax: Training and Inference

Training Input: Training data D_s , encoder f , density function $p(Z; \alpha)$, classifier g , learning rate η .

for $e = 1 \rightarrow$ epochs **do**

Sample D_B with a mini-batch B for source data D_s

$\theta_{g,f} \leftarrow \theta_{g,f} - \eta \nabla_{\theta_{g,f}} \mathbb{E}_{(x,y) \in D_B} [-y \log(\sigma(g(f(x))))]$

end for

$Z = f(X)$; **Do MLE** to yield $\hat{\alpha}$ in $p(Z; \alpha)$

Scale: $p(Z; \hat{\alpha})$ to $(0, 1]$

for $e = 1 \rightarrow$ re-optimize classifier epochs **do**

Sample D_B with a mini-batch B for source data D_s

$\theta_g \leftarrow \theta_g - \eta \nabla_{\theta_g} \mathbb{E}_{(z=f(x),y) \in D_B} [-y \log(\sigma(p(z; \hat{\alpha}) * g(z)))]$

end for

Inference Input: Test sample x_t

$z_t = f(x_t)$; $p(y = i | x_t) = \frac{\exp(p(z_t; \hat{\alpha}) * (z_t^\top \theta_{g_i}))}{\sum_{j=1}^K \exp(p(z_t; \hat{\alpha}) * (z_t^\top \theta_{g_j}))}, \forall i \in \mathcal{Y}$

The proof of Theorem 5.2 is provided in Appendix A.1. Theorem 5.2 shows that without density function, the standard softmax is non-uniform while Density-Softmax will provide a uniform distribution on OOD data. This is what we expect from Equation 5. Equation 5 also suggests that for IID data, we expect Density-Softmax follows the in-domain predictive distribution. Therefore, we next provide a theorem showing that the predictive distribution between in-domain softmax and Density-Softmax is the same on IID data by:

Theorem 5.3. (In-domain prediction for IID data). Consider x_{iid} and let the in-domain prediction of the softmax layer with the model which has already been learned from training data be: $\sigma(g(f(x_{iid})))$. Density-Softmax provides the same predictive distribution for x_{iid} by multiplication with a high likelihood value $p(z_{iid} = f(x_{iid}); \alpha) \rightarrow 1$, i.e.,

$$\sigma(p(z_{iid}; \alpha) * g(z_{iid})) = \sigma(g(f(x_{iid}))), \text{ where } z_{iid} = f(x_{iid}).$$

The proof of Theorem 5.3 is provided in Appendix A.2. Now, we know that Density-Softmax preserves the original predictive distribution for IID data and calibrates to uniform distribution for OOD data. Based on these two theorems, we next show that Density-Softmax is the solution of the minimax uncertainty risk in Equation 4 and satisfies Definition 3.2 about distance awareness by providing the following corollary and proposition:

Corollary 5.4. (Solution of the minimax uncertainty risk). If the predictive distribution of Density-Softmax follows Theorem 5.3 and Theorem 5.2, then Density-Softmax’s prediction is the optimal solution of the minimax uncertainty risk, i.e.,

$$\sigma(p(f(X); \alpha) * g(f(X))) = \arg \inf_{\mathbb{P}(Y|X) \in \mathcal{P}} \left[\sup_{\mathbb{P}^*(Y|X) \in \mathcal{P}^*} S(\mathbb{P}(Y|X), \mathbb{P}^*(Y|X)) \right].$$

The proof of Corollary 5.4 is provided in Appendix A.3.

Proposition 5.5. (Distance awareness). Consider the predictive distribution of Density-Softmax $\sigma(p(z = f(x); \alpha) * (g \circ f(x)))$, assume $f(x)$ satisfies distance preserving on latent space \mathcal{Z} , then $\sigma(p(z = f(x); \alpha) * (g \circ f(x)))$ is distance aware.

Proof sketch. We can prove Proposition 5.5 by showing (1) $p(z = f(x); \alpha)$ is monotonically decreasing w.r.t. distance $\mathbb{E} \|z_t - Z_s\|_{\mathcal{Z}}$ and (2) $p(z = f(x); \alpha) * g$ is distance aware. The full proof is provided in Appendix A.4. \square

Remark 5.6. Proposition 5.5 shows our Density-Softmax is distance awareness with a distance-preserving representation \mathcal{Z} , i.e., its predictive probability reflects the distance between the test sample and the training data. Regarding the distance-preserving assumption, we observe that doing ERM in the first step of Algorithm 1 gives a similar empirical result by making $f(x)$ distance-preserving on latent space \mathcal{Z} . On the other hand, it will cost more storage to enforce a distance-preserving representation because of needing to add Spectral-normalized layers. Therefore, in our practical algorithm, we do not explicitly enforce that. A detailed discussion is provided in Appendix B.2.

Following these results, we finally present Density-Softmax can enhance the uncertainty estimation quality of DNN with the standard softmax by reducing its over-confidence in the proposition below:

Proposition 5.7. (Reducing over-confidence of the standard softmax). If the predictive distribution of the standard softmax $\sigma(g \circ f)$ makes $\text{acc}(B_m) \leq \text{conf}(B_m), \forall B_m$, then Density-Softmax $\sigma((p(f; \alpha) * g) \circ f)$ can improve calibrated-uncertainty in terms of ECE (Equation 2), i.e.,

$$ECE(\sigma((p(f; \alpha) * g) \circ f)) \leq ECE(\sigma(g \circ f)).$$

The proof of Proposition 5.7 is provided in Appendix A.5.

Remark 5.8. The condition $\text{acc}(B_m) \leq \text{conf}(B_m), \forall B_m$ is a specific case of the over-confidence for every M bins. And if so, Proposition 5.7 shows our Density-Softmax can reduce ECE of the standard softmax, which also be empirically confirmed by reliability diagrams in Figure 5 in the next section.

6 Experiments

6.1 Experimental Settings

Datasets. We utilize 7 commonly used datasets under distributional shifts [5], including **Toy dataset** [11] with two moons and two ovals to visualize uncertainty and clustering. **CIFAR-10-C**, **CIFAR-100-C**, and **ImageNet-C** [68] for main benchmarking. To evaluate real-world shifts, we experiment on **SVHN** [69] for far domain OOD detection with CIFAR, **CIFAR-10.1** [70] for vision, and **CLINC OOS** [71] for language task. The detail of each dataset is provided in Appendix C.1.

Baseline. For a fair comparison, we use the fair and high-quality baseline of Nado et al. [5]. We compares with 13 recently SOTA methods in reliability, including **ERM** [21] is a standard deterministic, **ENN** [43], **Posterior Net** [24], **DUQ** [22], **DDU** [23, 40], **NUQ** [38], **SNGP** [11], probabilistic models contain **MC Dropout** [12], **DNN-GP** [10, 11], **MFVI BNN** [15, 16], **Rank-1 BNN** [18], and Ensembles families with **BatchEnsemble** [32] and **Deep Ensembles** [19, 20]. The detail of each method is provided in Appendix C.2.

Evaluation Metrics. To evaluate the predictive performance, we use NLL and Accuracy. For uncertainty estimation, we visualize uncertainty surfaces (entropy, different predictive variances), predictive entropy for distance awareness, AUPR/AUROC for OOD detection, and ECE with 15 bins for calibration. To compare the robustness under distributional shifts, we evaluate every OOD set in each dataset. To compare computational efficiency, we count the number of model parameters for storage requirements¹ and measure latency in milliseconds per sample for inference speed.

Implementation. We follow experimental settings based on the source code of Nado et al. [5]. We train models on the original train set, test on the original IID test, and aforementioned OOD sets. The performance is evaluated on backbones ResFFN-12-128 [11] for the toy dataset, Wide Resnet-28-10 [72] for CIFAR-10-100, Resnet-50 [73] for ImageNet, and BERT [74] for CLINC OOS dataset. We set all probabilistic models that require MC sampling and ensembling method equal to 4 for a fair computational comparison. Implementation details are provided in Appendix C.3. All source code to reproduce results are available at https://github.com/Angie-Lab-JHU/density_softmax.

6.2 Results

6.2.1 The quality of the uncertainty estimation

Density-Softmax achieves distance awareness. From Figure 1 on the two moons dataset, we observe that our model achieves distance awareness by having uniform class probability and high uncertainty value on OOD data, *confirming Proposition 5.5*. In particular, ERM, MC Dropout, Rank-1 BNN, and Ensembles can not provide distance awareness by no informative information about their variance for OOD data. Although SNGP shows distance awareness as well, it still makes confident predictions on OOD datapoints with around 0.0 variance. Meanwhile, our Density-Softmax provides an uncertainty estimate with the best-fit class probability for IID data and 1.0 variance on OOD. Similar observations are provided in Appendix C.4.1 with different uncertainty metrics and the different two ovals datasets.

We next show our method produces high entropy in OOD data and low entropy in IID data to achieve distance awareness. Figure 3 compares the density of predictive entropy between different methods trained on CIFAR-10 and tested on CIFAR-100. Because this is the semantic shift, we would expect the model to provide high entropy. Indeed, we observe that Density-Softmax achieves the highest entropy with a high-density value. In Figure 22 in Appendix C.4.4, we also observe that our model satisfies this condition in IID, confirming the hypothesis that our framework is distance aware. More details about histograms of each method and analysis are provided in Appendix C.4.4.

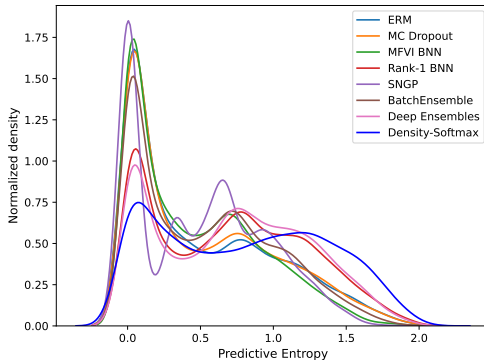


Figure 3: PDF plot of predictive entropy for the semantic shift, models are trained on CIFAR-10 and tested on CIFAR-100. **Density-Softmax provide highest entropy with high density for OOD.** Detailed figures are provided in Appendix C.4.4.

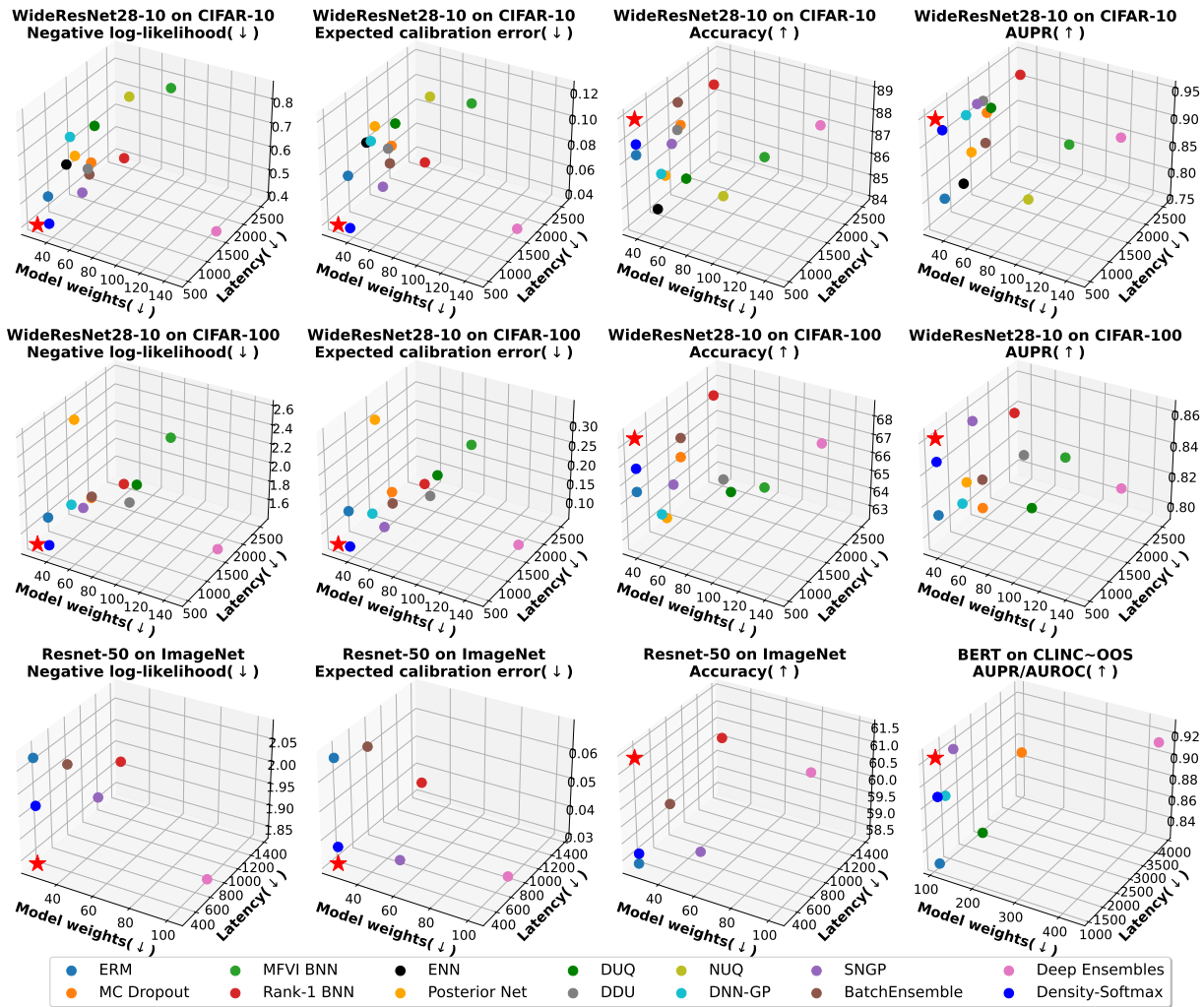


Figure 4: Results on average from the Table 3, 4, 5, and 6 in Appendix C.4.2 with z-axis represents the NLL, ECE (lower is better), accuracy, and AUPR/AUROC (higher are better). The x and y-axis represent model weights and latency (lower are better). **Red star** represents the desired corner. **Our Density-Softmax** always stay close to the **star**, indicating is the fastest, lightweight model, and has a competitive result with SOTA.

Density-Softmax has competitive uncertainty and robustness performances with SOTA. Table 3, 4, 5, and 6 in Appendix C.4.2 show benchmark results across shifted datasets. Figure 4 summarizes these tables on average per each criterion. From these results, we observe that our model has competitive performance and even sometimes outperforms the SOTA like Rank-1 BNN, SNGP, and Deep Ensembles, especially under OOD settings. E.g., in CIFAR-100-C, it *achieves the lowest cNLL and cECE with 2.20 and 0.102 respectively*, and is only slightly higher than SNGP and Deep Ensembles by 0.003 in cECE in ImageNet-C. Similarly, it *has the best AUPR-C with 0.801 in CIFAR-100, cNLL with 0.79 in CIFAR-10-C, and 0.015 oECE in CIFAR-10.1* and is only lower than Deep Ensembles by around 0.4% in accuracy in CIFAR-10. More details about benchmark comparison and analysis are provided in Appendix C.4.2, C.4.3, and C.4.4.

Density-Softmax archives competitive calibration performances with SOTA. To take a closer look at the calibration, we visualize reliability diagrams based on the ECE in Figure 5. We observe that our model is better calibrated than other methods in the real-world shifted OOD test set. E.g., compared to ERM, our model is less over-confident, *confirming Proposition 5.7*. Meanwhile, compared to Rank-1 BNN and Deep Ensembles, it is less under-confidence. More details about calibration with reliability diagrams of each method in both IID, OOD, and analysis are provided in Appendix C.4.3.

¹Unlike Nado et al. [5], Liu et al. [11]’s work that only counts trainable parameters, our paper reports the total of trainable and non-trainable for the number of model parameters in GPU. Regarding DDU [23, 40] which uses the post-hoc re-calibration, we only report its performance before the re-calibration step for a fair comparison.

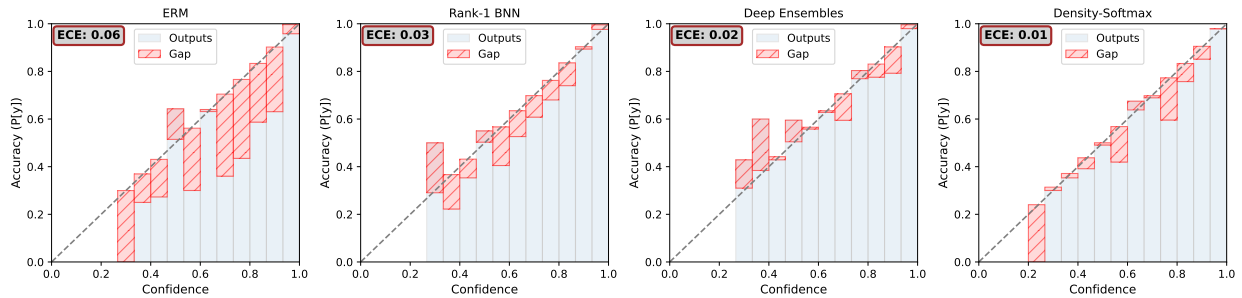


Figure 5: Reliability diagram of Density-Softmax v.s. different approaches, trained on CIFAR-10, test on CIFAR-10.1 (v6). **Density-Softmax is better-calibrated than others.** More figures are provided in Appendix C.4.3.

6.2.2 Scalability

Density-Softmax outperforms SOTA in inference speed. Our method only requires one forward pass to make a prediction, so it outperforms other SOTA in terms of inference speed. For every dataset with different backbones, we observe that Density-Softmax achieves almost the same latency with Deterministic-ERM. In particular, it takes less than 525, 300, and 1090 ms/sample in Wide Resnet-28-10, Resnet-50, and BERT for an inference. Having a similar latency, it is also more reliable than ERM by always archiving a lower NLL, ECE, and higher accuracy. E.g., in CIFAR-100, it achieves 0.780/81.2%/0.038 in NLL/Accuracy/ECE while ERM is only 0.875/79.8%/0.085 for IID test data. The gap is even significant in OOD where our model is better by 0.5/1.1%/0.137 respectively.

Density-Softmax outperforms SOTA in storage requirements. We also observe Density-Softmax is very lightweight with less than 36.65M, 25.88M, and 108.53M parameters in Wide Resnet-28-10, Resnet-50, and BERT correspondingly. As a result, combined with the latency performance, Density-Softmax outperforms other SOTA approaches in computational efficiency. In particular, our model is less than Deep Ensembles by 4 times in the number of parameters. Regarding the latency, compared with Rank-1 BNN, Density-Softmax is also lower than by around 6 times in latency.

6.2.3 Analysis of the density function

Our density model can capture distributional shifts.

An issue of the density estimation on high-dimensional samples like image pixels space \mathcal{X} is that the density function may provide the same likelihood value for IID and OOD data [24, 30, 66, 67]. To mitigate this issue, our Density-Softmax instead estimates on the lower-dimensional latent space \mathcal{Z} , which is fixed after doing ERM in the first step of Algorithm 1. This latent structure is therefore much simpler to estimate when compared to complex image pixels space \mathcal{X} . We visualize the likelihood histogram of our Flows density function across training, IID testing, and OOD sets in Figure 6. We observe that our density function provides a high likelihood for IID while low values for OOD test set. Importantly, when the shift intensity increase, the likelihood also decreases, showing our model can detect in-out-distribution data.

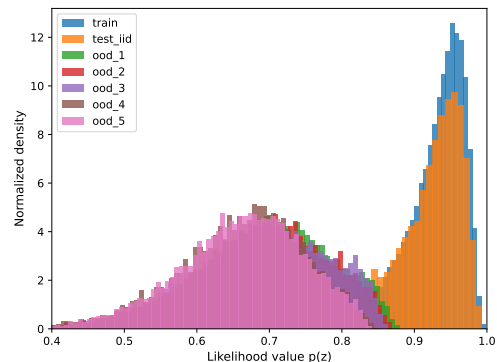


Figure 6: Histogram of the likelihood value $p(z; \alpha)$ from Flows model. **Blue** represents the likelihood of the CIFAR-10 train, **Orange** is IID test, **Green, Red, Purple, Brown, Pink** are OOD set from 1 to 5 shift intensity levels in CIFAR-10-C. **Our model provides high values on the IID test and lower values in OOD set w.r.t. intensity levels..**

7 Conclusion

Despite showing success in reliable machine learning, probabilistic methods like Deep Ensembles and BNN suffer from huge computational burdens. To tackle this challenge, we propose Density-Softmax, a fast and lightweight deterministic approach for uncertainty estimation under distribution shifts via a combination of a latent density function with the softmax layer. We complement this algorithm with a theoretical analysis establishing guarantees on in-out domain prediction, solution of the minimax uncertainty risk, distance awareness, and reducing over-confidence of the standard softmax. Empirically, we find our proposed framework achieves competitive results with SOTA methods in uncertainty estimation while outperforming them significantly in terms of memory and inference cost. For future work, we plan to tackle Density-Softmax’s limitations, including extending to regression tasks, improving estimation techniques to enhance the quality of the density function, and continuing to reduce the number of parameters to deploy this framework in real-world systems.

Acknowledgments

This work is supported by the JHU-Amazon AI2AI faculty award.

References

- [1] Andre Esteva, Alexandre Robicquet, Bharath Ramsundar, Volodymyr Kuleshov, Mark DePristo, Katherine Chou, Claire Cui, Greg Corrado, Sebastian Thrun, and Jeff Dean. A guide to deep learning in healthcare. *Nature Medicine*, 2019.
- [2] Jesse Levinson, Jake Askeland, Jan Becker, Jennifer Dolson, David Held, Soeren Kammel, J. Zico Kolter, Dirk Langer, Oliver Pink, Vaughan Pratt, Michael Sokolsky, Ganymed Stanek, David Stavens, Alex Teichman, Moritz Werling, and Sebastian Thrun. Towards fully autonomous driving: Systems and algorithms. In *2011 IEEE Intelligent Vehicles Symposium (IV)*, 2011.
- [3] Di Feng, Lars Rosenbaum, and Klaus Dietmayer. Towards safe autonomous driving: Capture uncertainty in the deep neural network for lidar 3d vehicle detection. In *2018 21st International Conference on Intelligent Transportation Systems (ITSC)*, 2018.
- [4] Chuan Guo, Geoff Pleiss, Yu Sun, and Kilian Q. Weinberger. On calibration of modern neural networks. In *Proceedings of the 34th International Conference on Machine Learning*, 2017.
- [5] Zachary Nado, Neil Band, Mark Collier, Josip Djolonga, Michael Dusenberry, Sebastian Farquhar, Angelos Filos, Marton Havasi, Rodolphe Jenatton, Ghassen Jerfel, Jeremiah Liu, Zelda Mariet, Jeremy Nixon, Shreyas Padhy, Jie Ren, Tim Rudner, Yeming Wen, Florian Wenzel, Kevin Murphy, D. Sculley, Balaji Lakshminarayanan, Jasper Snoek, Yarin Gal, and Dustin Tran. Uncertainty Baselines: Benchmarks for uncertainty & robustness in deep learning. *arXiv preprint arXiv:2106.04015*, 2021.
- [6] Yaniv Ovadia, Emily Fertig, Jie Ren, Zachary Nado, D. Sculley, Sebastian Nowozin, Joshua Dillon, Balaji Lakshminarayanan, and Jasper Snoek. Can you trust your model's uncertainty? evaluating predictive uncertainty under dataset shift. In *Advances in Neural Information Processing Systems*, 2019.
- [7] Dustin Tran, Jeremiah Liu, Michael W. Dusenberry, Du Phan, Mark Collier, Jie Ren, Kehang Han, Zi Wang, Zelda Mariet, Huiyi Hu, Neil Band, Tim G. J. Rudner, Karan Singhal, Zachary Nado, Joost van Amersfoort, Andreas Kirsch, Rodolphe Jenatton, Nithum Thain, Honglin Yuan, Kelly Buchanan, Kevin Murphy, D. Sculley, Yarin Gal, Zoubin Ghahramani, Jasper Snoek, and Balaji Lakshminarayanan. Plex: Towards reliability using pretrained large model extensions, 2022.
- [8] Matthias Minderer, Josip Djolonga, Rob Romijnders, Frances Hubis, Xiaohua Zhai, Neil Houlsby, Dustin Tran, and Mario Lucic. Revisiting the calibration of modern neural networks. In *Advances in Neural Information Processing Systems*, 2021.
- [9] Jacob Gardner, Geoff Pleiss, Kilian Q Weinberger, David Bindel, and Andrew G Wilson. Gpytorch: Blackbox matrix-matrix gaussian process inference with gpu acceleration. In *Advances in Neural Information Processing Systems*, 2018.
- [10] Jaehoon Lee, Jascha Sohl-dickstein, Jeffrey Pennington, Roman Novak, Sam Schoenholz, and Yasaman Bahri. Deep neural networks as gaussian processes. In *International Conference on Learning Representations*, 2018.
- [11] Jeremiah Liu, Zi Lin, Shreyas Padhy, Dustin Tran, Tania Bedrax Weiss, and Balaji Lakshminarayanan. Simple and principled uncertainty estimation with deterministic deep learning via distance awareness. In *Advances in Neural Information Processing Systems*, 2020.
- [12] Yarin Gal and Zoubin Ghahramani. Dropout as a bayesian approximation: Representing model uncertainty in deep learning. In *Proceedings of The 33rd International Conference on Machine Learning*, 2016.

- [13] Yarin Gal and Zoubin Ghahramani. A theoretically grounded application of dropout in recurrent neural networks. In *Advances in Neural Information Processing Systems*, 2016.
- [14] Yarin Gal, Jiri Hron, and Alex Kendall. Concrete dropout. In *Advances in Neural Information Processing Systems*, 2017.
- [15] Charles Blundell, Julien Cornebise, Koray Kavukcuoglu, and Daan Wierstra. Weight uncertainty in neural networks. In *Proceedings of the 32nd International Conference on Machine Learning*, 2015.
- [16] Yeming Wen, Paul Vicol, Jimmy Ba, Dustin Tran, and Roger Grosse. Flipout: Efficient pseudo-independent weight perturbations on mini-batches. In *International Conference on Learning Representations*, 2018.
- [17] Hippolyt Ritter, Aleksandar Botev, and David Barber. A scalable laplace approximation for neural networks. In *International Conference on Learning Representations*, 2018.
- [18] Michael Dusenberry, Ghassen Jerfel, Yeming Wen, Yian Ma, Jasper Snoek, Katherine Heller, Balaji Lakshminarayanan, and Dustin Tran. Efficient and scalable Bayesian neural nets with rank-1 factors. In *Proceedings of the 37th International Conference on Machine Learning*, 2020.
- [19] L.K. Hansen and P. Salamon. Neural network ensembles. *IEEE Transactions on Pattern Analysis and Machine Intelligence*, 1990.
- [20] Balaji Lakshminarayanan, Alexander Pritzel, and Charles Blundell. Simple and scalable predictive uncertainty estimation using deep ensembles. In *Advances in Neural Information Processing Systems*, 2017.
- [21] Vladimir N. Vapnik. *Statistical Learning Theory*. Wiley-Interscience, 1998.
- [22] Joost Van Amersfoort, Lewis Smith, Yee Whye Teh, and Yarin Gal. Uncertainty estimation using a single deep deterministic neural network. In *Proceedings of the 37th International Conference on Machine Learning*, 2020.
- [23] Jishnu Mukhoti, Joost van Amersfoort, Philip H. S. Torr, and Yarin Gal. Deep deterministic uncertainty for semantic segmentation. *CoRR*, 2021.
- [24] Bertrand Charpentier, Daniel Zügner, and Stephan Günnemann. Posterior network: Uncertainty estimation without ood samples via density-based pseudo-counts. In *Advances in Neural Information Processing Systems*, 2020.
- [25] Xin Dong, Junfeng Guo, Ang Li, Wei-Te Ting, Cong Liu, and H.T. Kung. Neural mean discrepancy for efficient out-of-distribution detection. In *Proceedings of the IEEE/CVF Conference on Computer Vision and Pattern Recognition (CVPR)*, 2022.
- [26] Natasa Tagasovska and David Lopez-Paz. Single-model uncertainties for deep learning. In *Advances in Neural Information Processing Systems*, 2019.
- [27] Jingkang Yang, Pengyun Wang, Dejian Zou, Zitang Zhou, Kunyuan Ding, Wenxuan Peng, Haoqi Wang, Guangyao Chen, Bo Li, Yiyun Sun, Xuefeng Du, Kaiyang Zhou, Wayne Zhang, Dan Hendrycks, Yixuan Li, and Ziwei Liu. Openood: Benchmarking generalized out-of-distribution detection. In *NeurIPS*, 2022.
- [28] Hongxin Wei, Renchunzi Xie, Hao Cheng, Lei Feng, Bo An, and Yixuan Li. Mitigating neural network overconfidence with logit normalization. In *International Conference on Machine Learning (ICML)*, 2022.
- [29] Volodymyr Kuleshov, Nathan Fenner, and Stefano Ermon. Accurate uncertainties for deep learning using calibrated regression. In *Proceedings of the 35th International Conference on Machine Learning*, 2018.
- [30] Volodymyr Kuleshov and Shachi Deshpande. Calibrated and sharp uncertainties in deep learning via density estimation. In *Proceedings of the 39th International Conference on Machine Learning*, 2022.

- [31] Henry Gouk, Eibe Frank, Bernhard Pfahringer, and Michael J. Cree. Regularisation of neural networks by enforcing lipschitz continuity. *Mach. Learn.*, 2021.
- [32] Yeming Wen, Dustin Tran, and Jimmy Ba. Batchensemble: an alternative approach to efficient ensemble and lifelong learning. In *International Conference on Learning Representations*, 2020.
- [33] Max Welling and Yee Whye Teh. Bayesian learning via stochastic gradient langevin dynamics. In *Proceedings of the 28th International Conference on International Conference on Machine Learning*, 2011.
- [34] Wesley J Maddox, Pavel Izmailov, Timur Garipov, Dmitry P Vetrov, and Andrew Gordon Wilson. A simple baseline for bayesian uncertainty in deep learning. In *Advances in Neural Information Processing Systems*, 2019.
- [35] Andrey Malinin and Mark Gales. Predictive uncertainty estimation via prior networks. In *Advances in Neural Information Processing Systems*, 2018.
- [36] Andrey Malinin and Mark Gales. Reverse kl-divergence training of prior networks: Improved uncertainty and adversarial robustness. In *Advances in Neural Information Processing Systems*, 2019.
- [37] Matthias Hein, Maksym Andriushchenko, and Julian Bitterwolf. Why relu networks yield high-confidence predictions far away from the training data and how to mitigate the problem. In *IEEE Conference on Computer Vision and Pattern Recognition*, 2019.
- [38] Nikita Kotelevskii, Aleksandr Artemenkov, Kirill Fedyanin, Fedor Noskov, Alexander Fishkov, Artem Shelmanov, Artem Vazhentsev, Aleksandr Petiushko, and Maxim Panov. Nonparametric uncertainty quantification for single deterministic neural network. In *Advances in Neural Information Processing Systems*, 2022.
- [39] Archit Karandikar, Nicholas Cain, Dustin Tran, Balaji Lakshminarayanan, Jonathon Shlens, Michael C Mozer, and Becca Roelofs. Soft calibration objectives for neural networks. In *Advances in Neural Information Processing Systems*, 2021.
- [40] Jishnu Mukhoti, Andreas Kirsch, Joost van Amersfoort, Philip H. S. Torr, and Yarin Gal. Deep deterministic uncertainty: A simple baseline, 2022.
- [41] Haoqi Wang, Zhizhong Li, Litong Feng, and Wayne Zhang. Vim: Out-of-distribution with virtual-logit matching. In *Proceedings of the IEEE/CVF Conference on Computer Vision and Pattern Recognition (CVPR)*, 2022.
- [42] Weitang Liu, Xiaoyun Wang, John Owens, and Yixuan Li. Energy-based out-of-distribution detection. In *Advances in Neural Information Processing Systems*, 2020.
- [43] Murat Sensoy, Lance Kaplan, and Melih Kandemir. Evidential deep learning to quantify classification uncertainty. In *Advances in Neural Information Processing Systems*, 2018.
- [44] Yibo Hu, Yuzhe Ou, Xujiang Zhao, Jin-Hee Cho, and Feng Chen. Multidimensional uncertainty-aware evidential neural networks. *Proceedings of the AAAI Conference on Artificial Intelligence*, 2021.
- [45] Carlos Riquelme, George Tucker, and Jasper Snoek. Deep bayesian bandits showdown: An empirical comparison of bayesian deep networks for thompson sampling. In *International Conference on Learning Representations*, 2018.
- [46] Jasper Snoek, Oren Rippel, Kevin Swersky, Ryan Kiros, Nadathur Satish, Narayanan Sundaram, Mostofa Patwary, Mr Prabhat, and Ryan Adams. Scalable bayesian optimization using deep neural networks. In *Proceedings of the 32nd International Conference on Machine Learning*, 2015.
- [47] Agustinus Kristiadi, Matthias Hein, and Philipp Hennig. Being bayesian, even just a bit, fixes overconfidence in ReLU networks. In *Proceedings of the 37th International Conference on Machine Learning*, 2020.

- [48] Haoxuan Wang, Anqi Liu, Zhiding Yu, Junchi Yan, Yisong Yue, and Anima Anandkumar. Distributionally robust learning for uncertainty calibration under domain shift, 2022.
- [49] Takeru Miyato, Toshiki Kataoka, Masanori Koyama, and Yuichi Yoshida. Spectral normalization for generative adversarial networks. In *International Conference on Learning Representations*, 2018.
- [50] A. P. Dawid. The well-calibrated bayesian. *Journal of the American Statistical Association*, 1982.
- [51] Hao Song, Tom Diethe, Meelis Kull, and Peter Flach. Distribution calibration for regression. In *Proceedings of the 36th International Conference on Machine Learning*, 2019.
- [52] Allan H. Murphy. A new vector partition of the probability score. *Journal of Applied Meteorology*, 1973.
- [53] Mahdi Pakdaman Naeni, Gregory F. Cooper, and Milos Hauskrecht. Obtaining well calibrated probabilities using bayesian binning. In *Proceedings of the Twenty-Ninth AAAI Conference on Artificial Intelligence*, 2015.
- [54] Tilmann Gneiting, Fadoua Balabdaoui, and Adrian E. Raftery. Probabilistic Forecasts, Calibration and Sharpness. *Journal of the Royal Statistical Society Series B: Statistical Methodology*, 2007.
- [55] Jeremy Nixon, Michael W Dusenberry, Linchuan Zhang, Ghassen Jerfel, and Dustin Tran. Measuring calibration in deep learning. In *CVPR Workshops*, 2019.
- [56] Peter L. Bartlett and Marten H. Wegkamp. Classification with a reject option using a hinge loss. *J. Mach. Learn. Res.*, 2008.
- [57] Danijar Hafner, Dustin Tran, Timothy Lillicrap, Alex Irpan, and James Davidson. Reliable uncertainty estimates in deep neural networks using noise contrastive priors, 2019.
- [58] Corinna Cortes, Mehryar Mohri, and Afshin Rostamizadeh. Learning non-linear combinations of kernels. In *Advances in Neural Information Processing Systems*, 2009.
- [59] Alexander Meinke and Matthias Hein. Towards neural networks that provably know when they don’t know. In *International Conference on Learning Representations*, 2020.
- [60] Tilmann Gneiting and Adrian E Raftery. Strictly proper scoring rules, prediction, and estimation. *Journal of the American Statistical Association*, 2007.
- [61] Jochen Bröcker. Reliability, sufficiency, and the decomposition of proper scores. *Quarterly Journal of the Royal Meteorological Society*, 2009.
- [62] Glenn W. Brier. Verification of Forecasts Expressed in Terms of Probability. *Monthly Weather Review*, 1950.
- [63] Walter J. Scheirer, Lalit P. Jain, and Terrance E. Boult. Probability models for open set recognition. *IEEE Transactions on Pattern Analysis and Machine Intelligence*, 2014.
- [64] Emanuel Parzen. On Estimation of a Probability Density Function and Mode. *The Annals of Mathematical Statistics*, 1962.
- [65] Laurent Dinh, Jascha Sohl-Dickstein, and Samy Bengio. Density estimation using real NVP. In *International Conference on Learning Representations*, 2017.
- [66] George Papamakarios, Eric Nalisnick, Danilo Jimenez Rezende, Shakir Mohamed, and Balaji Lakshminarayanan. Normalizing flows for probabilistic modeling and inference. *Journal of Machine Learning Research*, 2021.
- [67] Eric Nalisnick, Akihiro Matsukawa, Yee Whye Teh, Dilan Gorur, and Balaji Lakshminarayanan. Do deep generative models know what they don’t know? In *International Conference on Learning Representations*, 2019.

- [68] Dan Hendrycks and Thomas Dietterich. Benchmarking neural network robustness to common corruptions and perturbations. In *International Conference on Learning Representations*, 2019.
- [69] Yuval Netzer, Tao Wang, Adam Coates, Alessandro Bissacco, Bo Wu, and Andrew Y. Ng. Reading digits in natural images with unsupervised feature learning. In *NIPS Workshop on Deep Learning and Unsupervised Feature Learning 2011*, 2011.
- [70] Benjamin Recht, Rebecca Roelofs, Ludwig Schmidt, and Vaishal Shankar. Do cifar-10 classifiers generalize to cifar-10?, 2018.
- [71] Stefan Larson, Anish Mahendran, Joseph J. Peper, Christopher Clarke, Andrew Lee, Parker Hill, Jonathan K. Kummerfeld, Kevin Leach, Michael A. Laurenzano, Lingjia Tang, and Jason Mars. An evaluation dataset for intent classification and out-of-scope prediction. In *Proceedings of the 2019 Conference on Empirical Methods in Natural Language Processing and the 9th International Joint Conference on Natural Language Processing (EMNLP-IJCNLP)*, 2019.
- [72] Sergey Zagoruyko and Nikos Komodakis. Wide residual networks. In *Proceedings of the British Machine Vision Conference (BMVC)*, 2016.
- [73] Kaiming He, Xiangyu Zhang, Shaoqing Ren, and Jian Sun. Deep residual learning for image recognition. In *2016 IEEE Conference on Computer Vision and Pattern Recognition (CVPR)*, 2016.
- [74] Jacob Devlin, Ming-Wei Chang, Kenton Lee, and Kristina Toutanova. BERT: Pre-training of deep bidirectional transformers for language understanding. In *Proceedings of the 2019 Conference of the North American Chapter of the Association for Computational Linguistics: Human Language Technologies, Volume 1 (Long and Short Papers)*, 2019.
- [75] Peter D. Grünwald and A. Philip Dawid. Game theory, maximum entropy, minimum discrepancy and robust Bayesian decision theory. *The Annals of Statistics*, 2004.
- [76] Matthew Parry, A. Philip Dawid, and Steffen Lauritzen. Proper local scoring rules. *The Annals of Statistics*, 2012.
- [77] Mícheál O. Searcóid. *Metric Spaces*. Springer London, London, 2007 edition edition, August 2006. ISBN 978-1-84628-369-7.
- [78] Alex Krizhevsky and Geoffrey Hinton. Learning multiple layers of features from tiny images. Technical report, University of Toronto, 2009.
- [79] Antonio Torralba, Rob Fergus, and William T. Freeman. 80 million tiny images: A large data set for nonparametric object and scene recognition. *IEEE Transactions on Pattern Analysis and Machine Intelligence*, 2008.
- [80] Jia Deng, Wei Dong, Richard Socher, Li-Jia Li, Kai Li, and Li Fei-Fei. Imagenet: A large-scale hierarchical image database. In *2009 IEEE Conference on Computer Vision and Pattern Recognition*, 2009.
- [81] Dan Hendrycks*, Norman Mu*, Ekin Dogus Cubuk, Barret Zoph, Justin Gilmer, and Balaji Lakshminarayanan. Augmix: A simple method to improve robustness and uncertainty under data shift. In *International Conference on Learning Representations*, 2020.
- [82] Diederik P. Kingma and Jimmy Ba. Adam: A method for stochastic optimization. In *3rd International Conference on Learning Representations, ICLR 2015, San Diego, CA, USA, May 7-9, 2015, Conference Track Proceedings*, 2015.
- [83] Yangyi Chen, Lifan Yuan, Ganqu Cui, Zhiyuan Liu, and Heng Ji. A close look into the calibration of pre-trained language models, 2022.

Acronyms

AUPR Area Under the Precision-Recall.

AUROC Area Under the Receiver Operating Characteristic.

BERT Bidirectional Encoder Representations from Transformers.

BNN Bayesian Neural Network.

DDU Deep Deterministic Uncertainty.

DNN Deep Neural Network.

DNN-GP Deep Neural Network-Gaussian Process.

DUQ Deterministic Uncertainty Quantification.

ECE Expected Calibration Error.

ENN Evidential Neural Network.

ERM Empirical Risk Minimization.

IID Independent-identically-distributed.

KDE Kernel Density Estimation.

KNN K-Nearest Neighbors.

MC Monte-Carlo.

MFVI Mean-Field Variational Inference.

MLE Maximum Likelihood Estimation.

NLL Negative log-likelihood.

NUQ Nonparametric Uncertainty Quantification.

OOD Out-of-Distribution.

SNGP Spectral-normalized Neural Gaussian Process.

SOTA State-of-the-art.

Density-Softmax: Scalable and Calibrated Uncertainty Estimation under Distribution Shifts (Supplementary Material)

In this supplementary material, we collect proofs and remaining materials that were deferred from the main paper.

- In Appendix A, we provide the proofs for all the results in the main paper, including proof of Theorem 5.2 in Appendix A.1, proof of Theorem 5.3 in Appendix A.2, proof of Corollary 5.4 in Appendix A.3, proof of Proposition 5.5 in Appendix A.4, and proof of Proposition 5.7 in Appendix A.5.
- In Appendix B, we make further discussions and ablation studies about our method, including a discussion about density estimation and likelihood value implementation in Appendix B.1, and distance preserving assumption on latent space in Appendix B.2.
- In Appendix C, we provide additional information about our experiments, including sufficient details about the dataset in Appendix C.1, baseline details in Appendix C.2, implementation details to reproduce our experiments in Appendix C.3, and further empirical analysis and additional results in Appendix C.4.
The additional results in Appendix C.4 contains result for the toy dataset in Appendix C.4.1, result for benchmark dataset in Appendix C.4.2, uncertainty details about calibration in Appendix C.4.3, and about predictive entropy in Appendix C.4.4.

A Proofs

In this appendix, we provide proof of the theoretical results from the main paper.

A.1 Proof of Theorem 5.2

Proof. By assuming the non-uniform in predictive distribution $\sigma(g(f(x_{ood}))) \neq \mathbb{U}$, we have

$$p(y = i | x_{ood}) = \frac{\exp(z_{ood}^\top \theta_{g_i})}{\sum_{j=1}^K \exp(z_{ood}^\top \theta_{g_j})} \neq \frac{1}{K}, \forall i \in \mathcal{Y}, \quad (11)$$

where $z_{ood} = f(x_{ood})$ is the latent presentation for test sample x_{ood} , K is the total of the number of categorical in the discrete label space \mathcal{Y} .

Consider Density-Softmax predictive distribution $\sigma(p(z_{ood}; \alpha) * g(z_{ood}))$, we have

$$p(y = i | x_{ood}) = \frac{\exp(p(z_{ood}; \alpha) * (z_{ood}^\top \theta_{g_i}))}{\sum_{j=1}^K \exp(p(z_{ood}; \alpha) * (z_{ood}^\top \theta_{g_j}))}, \forall i \in \mathcal{Y}. \quad (12)$$

Due to x_{ood} is OOD data, then $x_{ood} \in D_t$, where $D_t \stackrel{iid}{\sim} \mathbb{P}_t(X, Y)$ and $\mathbb{P}_t(X, Y) \neq \mathbb{P}_s(X, Y)$ since Distributional Shift. By assuming a low likelihood for x_{ood} on latent space \mathcal{Z} in Assumption 5.1, i.e., $p(z_{ood}; \alpha) \rightarrow 0$, where $z_{ood} = f(x_{ood})$, then

$$\lim_{p(z_{ood}; \alpha) \rightarrow 0} \exp(p(z_{ood}; \alpha) * (z_{ood}^\top \theta_{g_i})) = e^0 = 1, \forall i \in \mathcal{Y}. \quad (13)$$

Since $\exp(p(z_{ood}; \alpha) * (z_{ood}^\top \theta_{g_j})) = 1, \forall j \in \mathcal{Y}$ when $p(z_{ood}; \alpha) \rightarrow 0$, then

$$p(y = i | x_{ood}) = \frac{\exp(p(z_{ood}; \alpha) * (z_{ood}^\top \theta_{g_i}))}{\sum_{j=1}^K \exp(p(z_{ood}; \alpha) * (z_{ood}^\top \theta_{g_j}))} = \frac{1}{\sum_{i=1}^K 1} = \frac{1}{K}, \forall i \in \mathcal{Y}. \quad (14)$$

As a consequence, we obtain the conclusion: $\sigma(p(z_{ood}; \alpha) * g(z_{ood})) = \mathbb{U}$, where \mathbb{U} stands for uniform distribution of Theorem 5.2. \square

A.2 Proof of Theorem 5.3

Proof. Consider Density-Softmax predictive distribution $\sigma(p(z_{iid}; \alpha) * g(z_{iid}))$, where $z_{iid} = f(x_{iid})$. We have

$$p(y = i | x_{iid}) = \frac{\exp(p(z_{iid}; \alpha) * (z_{iid}^\top \theta_{g_i}))}{\sum_{j=1}^K \exp(p(z_{iid}; \alpha) * (z_{iid}^\top \theta_{g_j}))}, \forall i \in \mathcal{Y}. \quad (15)$$

Due to x_{iid} is IID test data, then $x_{iid} \in D_t$, where $D_t \stackrel{iid}{\sim} \mathbb{P}_t(X, Y)$ and $\mathbb{P}_t(X, Y) = \mathbb{P}_s(X, Y)$. By assuming a high likelihood for x_{iid} on latent space \mathcal{Z} in Assumption 5.1, i.e., $p(z_{iid}; \alpha) \rightarrow 1$, where $z_{iid} = f(x_{iid})$, then

$$\lim_{p(z_{iid}; \alpha) \rightarrow 1} \exp(p(z_{iid}; \alpha) * (z_{iid}^\top \theta_{g_i})) = \exp(z_{iid}^\top \theta_{g_i}), \forall i \in \mathcal{Y}. \quad (16)$$

Since $\exp(p(z_{iid}; \alpha) * (z_{iid}^\top \theta_{g_i})) = \exp(z_{iid}^\top \theta_{g_i}), \forall i \in \mathcal{Y}$ when $p(z_{iid}; \alpha) \rightarrow 1$, then

$$p(y = i | x_{iid}) = \frac{\exp(p(z_{iid}; \alpha) * (z_{iid}^\top \theta_{g_i}))}{\sum_{j=1}^K \exp(p(z_{iid}; \alpha) * (z_{iid}^\top \theta_{g_j}))} = \frac{\exp(z_{iid}^\top \theta_{g_i})}{\sum_{j=1}^K \exp(z_{iid}^\top \theta_{g_j})}, \forall i \in \mathcal{Y}. \quad (17)$$

As a consequence, we obtain the conclusion: $\sigma(p(z_{iid}; \alpha) * g(z_{iid})) = \sigma(g(f(x_{iid})))$ of Theorem 5.3. \square

A.3 Proof of Corollary 5.4

Proof. This proof is based on the following provable Lemma of Liu et al. [11]:

Lemma A.1. [11, 75] (*The uniform distribution \mathbb{U} is the optimal for minimax Bregman score in $x \notin \mathcal{X}_{iid}$*). Consider the Bregman score [76] as follows

$$s(p, p^* | x) = \sum_{k=1}^K \{ [p^*(y_k|x) - p(y_k|x)] \psi'(p^*(y_k|x)) - \psi(p^*(y_k|x)) \},$$

where ψ is a strictly concave and differentiable function. Bregman score reduces to the log score when $\psi(p) = p \log(p)$, and reduces to the Brier score when $\psi(p) = p^2 - \frac{1}{K}$.

So, let consider the strictly proper scoring rules $S(\mathbb{P}(Y|X), \mathbb{P}^*(Y|X))$ [60, 61], since $\mathbb{P}(Y|X)$ is predictive, and $\mathbb{P}^*(Y|X)$ is the data-generation distribution, then for $\mathcal{X}_{ood} = \mathcal{X} / \mathcal{X}_{iid}$, using the result from Liu et al. [11], we have

$$S(\mathbb{P}, \mathbb{P}^*) = \mathbb{E}_{x \sim X} (s(p, p^* | x)) = \int_{\mathcal{X}} s(p, p^* | x) p^*(x) dx \quad (18)$$

$$= \int_{\mathcal{X}} s(p, p^* | x) [p^*(x|x \in \mathcal{X}_{iid}) p^*(x \in \mathcal{X}_{iid}) + p^*(x|x \in \mathcal{X}_{ood}) p^*(x \in \mathcal{X}_{ood})] dx \quad (19)$$

$$= \underbrace{\mathbb{E}_{x \sim \mathcal{X}_{iid}} (s(p, p^* | x))}_{S_{iid}(\mathbb{P}, \mathbb{P}^*)} p^*(x \in \mathcal{X}_{iid}) + \underbrace{\mathbb{E}_{x \sim \mathcal{X}_{ood}} (s(p, p^* | x))}_{S_{ood}(\mathbb{P}, \mathbb{P}^*)} p^*(x \in \mathcal{X}_{ood}). \quad (20)$$

Therefore, since $S_{iid}(\mathbb{P}, \mathbb{P}^*)$ and $S_{ood}(\mathbb{P}, \mathbb{P}^*)$ has disjoint support, we have the minimax uncertainty risk in Equation 4 equivalents to

$$\inf_{\mathbb{P}} \sup_{\mathbb{P}^*} S(\mathbb{P}, \mathbb{P}^*) = \inf_{\mathbb{P}} \left[\sup_{\mathbb{P}^*} [S_{iid}(\mathbb{P}, \mathbb{P}^*) * \mathbb{P}^*(\mathcal{X}_{iid})] + \sup_{\mathbb{P}^*} [S_{ood}(\mathbb{P}, \mathbb{P}^*) * \mathbb{P}^*(\mathcal{X}_{ood})] \right] \quad (21)$$

$$= \inf_{\mathbb{P}} \sup_{\mathbb{P}^*} [S_{iid}(\mathbb{P}, \mathbb{P}^*) * \mathbb{P}^*(\mathcal{X}_{iid})] + \inf_{\mathbb{P}} \sup_{\mathbb{P}^*} [S_{ood}(\mathbb{P}, \mathbb{P}^*) * \mathbb{P}^*(\mathcal{X}_{ood})]. \quad (22)$$

Due to $\mathbb{P}(Y|X_{iid})$ is the predictive distribution learned from data, we obtain $\inf_{\mathbb{P}} \sup_{\mathbb{P}^*} [S_{iid}(\mathbb{P}, \mathbb{P}^*)]$ is fixed and Density-Softmax satisfy by $\sigma(p(f(x_{iid}); \alpha) * g(f(x_{iid}))) = \sigma(g(f(x_{iid})))$ in Theorem 5.3 and Proof A.2. On the other hand, we have

$$\sup_{\mathbb{P}^* \in \mathcal{P}^*} [S_{ood}(\mathbb{P}, \mathbb{P}^*)] = \mathbb{E}_{x \sim X_{ood}} \sup_{p^*} [s(p, p^* | x)] p(x). \quad (23)$$

Applying the result from Lemma A.1 and combining with the result from Theorem 5.2 and Proof A.1, we obtain

$$\sigma(p(f(x_{ood}); \alpha) * g(f(x_{ood}))) = \mathbb{U} = \arg \inf_{\mathbb{P} \in \mathcal{P}} \sup_{\mathbb{P}^* \in \mathcal{P}^*} [S_{ood}(\mathbb{P}, \mathbb{P}^*)]. \quad (24)$$

As a consequence, we obtain the conclusion: Density-Softmax's prediction is the optimal solution of the minimax uncertainty risk, i.e.,

$$\sigma(p(f(X); \alpha) * g(f(X))) = \arg \inf_{\mathbb{P}(Y|X) \in \mathcal{P}} \left[\sup_{\mathbb{P}^*(Y|X) \in \mathcal{P}^*} S(\mathbb{P}(Y|X), \mathbb{P}^*(Y|X)) \right] \quad (25)$$

of Corollary 5.4. □

A.4 Proof of Proposition 5.5

Proof. The proofs contain three parts. The first part is showing density function $p(z_t; \alpha)$ is monotonically decreasing w.r.t. distance function $\mathbb{E} \|z_t - Z_s\|_{\mathcal{Z}}$. The second part is showing the metric $u(x_t)$ is maximized if $p(z_t; \alpha) \rightarrow 0$. The third part is showing $u(x_t)$ monotonically decreasing w.r.t. $p(z_t; \alpha)$ on the interval $(0, 1]$.

Part (1). The monotonic decrease of density function $p(z_t; \alpha)$ w.r.t. distance function $\mathbb{E} \|z_t - Z_s\|_{\mathcal{Z}}$: Consider the probability density function $p(z_t; \alpha)$ follows the Gaussian distribution with mean (median) μ and standard deviation σ , then we have

$$p(z_t; \alpha) = \frac{1}{\sigma\sqrt{2\pi}} \exp\left(\frac{-1}{2} \left(\frac{z_t - \mu}{\sigma}\right)^2\right). \quad (26)$$

Take derivative, we obtain

$$\frac{d}{dz_t} p(z_t; \alpha) = \left[\frac{-1}{2} \left(\frac{z_t - \mu}{\sigma}\right)^2 \right]' p(z_t; \alpha) = \frac{\mu - z_t}{\sigma^2} p(z_t; \alpha) \Rightarrow \begin{cases} \frac{d}{dz_t} p(z_t; \alpha) > 0 & \text{if } z_t < \mu, \\ \frac{d}{dz_t} p(z_t; \alpha) = 0 & \text{if } z_t = \mu, \\ \frac{d}{dz_t} p(z_t; \alpha) < 0 & \text{if } z_t > \mu. \end{cases} \quad (27)$$

Consider the distance function $\mathbb{E} \|z_t - Z_s\|_{\mathcal{Z}}$ follows the absolute norm, then we have

$$\mathbb{E} \|z_t - Z_s\|_{\mathcal{Z}} = \mathbb{E} (|z_t - Z_s|) = \int_{-\infty}^{z_t} \mathbb{P}(Z_s \leq t) dt + \int_{z_t}^{+\infty} \mathbb{P}(Z_s \geq t) dt. \quad (28)$$

Take derivative, we obtain

$$\frac{d}{dz_t} \mathbb{E} \|z_t - Z_s\|_{\mathcal{Z}} = \mathbb{P}(Z_s \leq z_t) - \mathbb{P}(Z_s \geq z_t) \Rightarrow \begin{cases} \frac{d}{dz_t} \mathbb{E} \|z_t - Z_s\|_{\mathcal{Z}} < 0 & \text{if } z_t < \mu, \\ \frac{d}{dz_t} \mathbb{E} \|z_t - Z_s\|_{\mathcal{Z}} = 0 & \text{if } z_t = \mu, \\ \frac{d}{dz_t} \mathbb{E} \|z_t - Z_s\|_{\mathcal{Z}} > 0 & \text{if } z_t > \mu. \end{cases} \quad (29)$$

Combining the result in Equation 27 and Equation 29, we have $p(z_t; \alpha)$ is maximized when $\mathbb{E} \|z_t - Z_s\|_{\mathcal{Z}}$ is minimized at the median μ , $p(z_t; \alpha)$ increase when $\mathbb{E} \|z_t - Z_s\|_{\mathcal{Z}}$ decrease and vice versa. As a consequence, we obtain $p(z_t; \alpha)$ is monotonically decreasing w.r.t. distance function $\mathbb{E} \|z_t - Z_s\|_{\mathcal{Z}}$.

Part (2). The maximum of metric $u(x_t)$: Consider $u(x_t) = v(d(x_t, X_s))$ in Definition 3.2, let $u(x_t)$ is the entropy of predictive distribution of Density-Softmax $\sigma(p(z = f(x); \alpha) * (g \circ f(x)))$, then we have

$$u(x_t) = H(\sigma(p(z_t; \alpha) * g(z_t))) \quad (30)$$

$$= - \sum_{i=1}^K p(y = i | \sigma(p(z_t; \alpha) * g(z_t))) \log(p(y = i | \sigma(p(z_t; \alpha) * g(z_t)))) \quad (31)$$

$$= - \sum_{i=1}^K \frac{\exp(p(z_t; \alpha) * (z_t^\top \theta_{g_i}))}{\sum_{j=1}^K \exp(p(z_t; \alpha) * (z_t^\top \theta_{g_j}))} \log \left(\frac{\exp(p(z_t; \alpha) * (z_t^\top \theta_{g_i}))}{\sum_{j=1}^K \exp(p(z_t; \alpha) * (z_t^\top \theta_{g_j}))} \right). \quad (32)$$

Let $a_i = \frac{\exp(p(z_t; \alpha) * (z_t^\top \theta_{g_i}))}{\sum_{j=1}^K \exp(p(z_t; \alpha) * (z_t^\top \theta_{g_j}))}$, then we need to find

$$(a_1, \dots, a_K) \text{ to maximize } - \sum_{i=1}^K (a_i) \log(a_i) \text{ subject to } \sum_{i=1}^K (a_i) - 1 = 0. \quad (33)$$

Since $-\sum_{i=1}^K (a_i) \log(a_i)$ is an entropy function, it strictly concave on \vec{a} . In addition, because the constraint is $\sum_{i=1}^K (a_i) - 1 = 0$, the Mangasarian-Fromovitz constraint qualification holds. So, apply the Lagrange multiplier, we have the Lagrange function

$$\mathcal{L}(a_1, \dots, a_K, \lambda) = - \sum_{i=1}^K (a_i) \log(a_i) - \lambda \left(\sum_{i=1}^K (a_i) - 1 \right). \quad (34)$$

Calculate the gradient, and we obtain

$$\nabla_{a_1, \dots, a_K, \lambda} \mathcal{L}(a_1, \dots, a_K, \lambda) = \left(\frac{\partial \mathcal{L}}{\partial a_1}, \dots, \frac{\partial \mathcal{L}}{\partial a_K}, \frac{\partial \mathcal{L}}{\partial \lambda} \right) \quad (35)$$

$$= \left(-(\log(a_1) + \frac{1}{a_1}) - \lambda, \dots, -(\log(a_K) + \frac{1}{a_K}) - \lambda, \sum_{i=1}^K (a_i) - 1 \right), \quad (36)$$

and therefore

$$\nabla_{a_1, \dots, a_K, \lambda} \mathcal{L}(a_1, \dots, a_K, \lambda) = 0 \Leftrightarrow \begin{cases} -(\log(a_i) + \frac{1}{a_i}) - \lambda = 0, \forall i \in \mathcal{Y}, \\ \sum_{i=1}^K (a_i) - 1 = 0. \end{cases} \quad (37)$$

Consider $-(\log(a_i) + \frac{1}{a_i}) - \lambda = 0, \forall i \in \mathcal{Y}$, this shows that all a_i are equal (because they depend on λ only). By using $\sum_{i=1}^K (a_i) - 1 = 0$, we find

$$a_i = \frac{\exp(p(z_t; \alpha) * (z_t^\top \theta_{g_i}))}{\sum_{j=1}^K \exp(p(z_t; \alpha) * (z_t^\top \theta_{g_j}))} = \frac{1}{K}, \forall i \in \mathcal{Y}. \quad (38)$$

As a consequence, $u(x_t)$ is maximized if the predictive distribution $\sigma(p(z = f(x); \alpha) * (g \circ f(x))) = \mathbb{U}$, i.e., $p(z_t; \alpha) \rightarrow 0$ which will happen if z_t is OOD data (since the result in Theorem 5.2 and Proof A.1).

Part (3). The monotonically decrease of metric $u(x_t)$ on the interval $(0, 1]$: Consider the function

$$\mathcal{F}(p(z_t; \alpha)) = - \sum_{i=1}^K \frac{\exp(p(z_t; \alpha) * (z_t^\top \theta_{g_i}))}{\sum_{j=1}^K \exp(p(z_t; \alpha) * (z_t^\top \theta_{g_j}))} \log \left(\frac{\exp(p(z_t; \alpha) * (z_t^\top \theta_{g_i}))}{\sum_{j=1}^K \exp(p(z_t; \alpha) * (z_t^\top \theta_{g_j}))} \right). \quad (39)$$

Let $a = p(z_t; \alpha)$, $b_i = z_t^\top \theta_{g_i}, \forall i \in \mathcal{Y}$ then

$$\mathcal{F}(a) = - \sum_{i=1}^K \frac{e^{ab_i}}{\sum_{j=1}^K e^{ab_j}} \log \left(\frac{e^{ab_i}}{\sum_{j=1}^K e^{ab_j}} \right), \quad (40)$$

and we need to find $\frac{d}{da}\mathcal{F}$.

Take derivative, we obtain

$$\frac{d}{da}\mathcal{F} = -\sum_{i=1}^K \left\{ \left(\frac{e^{ab_i}}{\sum_{j=1}^K e^{ab_j}} \right)' \log \left(\frac{e^{ab_i}}{\sum_{j=1}^K e^{ab_j}} \right) + \frac{e^{ab_i}}{\sum_{j=1}^K e^{ab_j}} \left[\log \left(\frac{e^{ab_i}}{\sum_{j=1}^K e^{ab_j}} \right) \right]' \right\} \quad (41)$$

$$= -\sum_{i=1}^K \left[\left(\frac{e^{ab_i}}{\sum_{j=1}^K e^{ab_j}} \right)' \log \left(\frac{e^{ab_i}}{\sum_{j=1}^K e^{ab_j}} \right) + \frac{e^{ab_i}}{\sum_{j=1}^K e^{ab_j}} \left(\frac{e^{ab_i}}{\sum_{j=1}^K e^{ab_j}} \right)' \frac{\sum_{j=1}^K e^{ab_j}}{e^{ab_i}} \right] \quad (42)$$

$$= -\sum_{i=1}^K \left\{ \frac{b_i e^{ab_i} \sum_{j=1}^K e^{ab_j} - e^{ab_i} \sum_{j=1}^K b_j e^{ab_j}}{(\sum_{j=1}^K e^{ab_j})^2} \left[\log \left(\frac{e^{ab_i}}{\sum_{j=1}^K e^{ab_j}} \right) + 1 \right] \right\} \quad (43)$$

$$= -\sum_{i=1}^K \left\{ \frac{\sum_{j=1}^K e^{a(b_i+b_j)} (b_i - b_j)}{(\sum_{j=1}^K e^{ab_j})^2} \left[\log \left(\frac{e^{ab_i}}{\sum_{j=1}^K e^{ab_j}} \right) + 1 \right] \right\}. \quad (44)$$

By assuming the non-uniform in the predictive distribution $\sigma(g(f(x_{ood}))) \neq \mathbb{U}$ and $a \in (0, 1]$, then

$$\frac{d}{da}\mathcal{F} = -\sum_{i=1}^K \left\{ \frac{\sum_{j=1}^K e^{a(b_i+b_j)} (b_i - b_j)}{(\sum_{j=1}^K e^{ab_j})^2} \left[\log \left(\frac{e^{ab_i}}{\sum_{j=1}^K e^{ab_j}} \right) + 1 \right] \right\} < 0, \quad (45)$$

combining with $u(x_t)$ is maximized if $a \rightarrow 0$, we obtain $u(x_t)$ decrease monotonically on the interval $(0, 1]$.

Combining the result in *Part (2)*. $u(x_t)$ is maximized if $p(z_t; \alpha) \rightarrow 0$ which will happen if z_t is OOD data, and the result in *Part (3)*. $u(x_t)$ is decrease monotonically w.r.t. $p(z_t; \alpha)$ on the interval $(0, 1]$ which will happen if x_t is closer to IID data since the likelihood value $p(z_t; \alpha)$ increases, we obtain the distance awareness of $p(z = f(x); \alpha) * g$.

Combining the result in *Part (1)*. $p(z_t; \alpha)$ is monotonically decreasing w.r.t. distance function $\mathbb{E} \|z_t - Z_s\|_{\mathcal{Z}}$, and the result *distance awareness* of $p(z = f(x); \alpha) * g$ and the assumption that $f(x)$ satisfies *distance preserving* on latent space \mathcal{Z} , we obtain the conclusion: $\sigma(p(z = f(x); \alpha) * (g \circ f(x)))$ is distance awareness of Proposition 5.5. \square

A.5 Proof of Proposition 5.7

Proof. Consider the predictive distribution of the standard softmax $\sigma(g(f(x)))$. By definition, we have

$$\begin{aligned} \sigma : \quad \mathbb{R}^K &\rightarrow \Delta_y \\ g(f(x)) &\mapsto \sigma(g(f(x))). \end{aligned}$$

Let the logit vectors of $g(f(x))$ be $u = (u_1, \dots, u_K) \in \mathbb{R}^K$, for an arbitrary pair of classes, i.e., $\forall i, j \in \{1, \dots, K\}$ of the logit vector u , assume that $u_i < u_j$. Since the predictive distribution of Density-Softmax is $\sigma(p(f(x); \alpha) * g(f(x)))$, we have the corresponding logit vector is

$$p(f(x); \alpha) * u = (p(f(x); \alpha) * u_1, \dots, p(f(x); \alpha) * u_K) \in \mathbb{R}^K. \quad (46)$$

Due to $p(f(x); \alpha) \in (0, 1]$, then we obtain the following relationship holds

$$[p(f(x); \alpha) * u]_i < [p(f(x); \alpha) * u]_j, \quad (47)$$

where $[\cdot]_i$ represents the i -th entry of the vector. Since the order of entries in the logit vector is unchanged between the standard softmax and Density-Softmax, we obtain

$$\arg \max_{y \in \mathcal{Y}} [\sigma(g(f(x)))]_y = \arg \max_{y \in \mathcal{Y}} [\sigma(p(f(x); \alpha) * g(f(x)))]_y. \quad (48)$$

As a consequence, Density-Softmax preserves the classification accuracy of the standard softmax by

$$\text{acc}(B_m) = \frac{1}{|B_m|} \sum_{i \in B_m} \mathbb{I}(\arg \max_{y \in \mathcal{Y}} [\sigma(g(f(x_i)))]_y = y_i) \quad (49)$$

$$= \frac{1}{|B_m|} \sum_{i \in B_m} \mathbb{I}(\arg \max_{y \in \mathcal{Y}} [\sigma(p(f(x_i); \alpha) * g(f(x_i)))]_y = y_i), \quad (50)$$

where B_m is the set of sample indices whose confidence falls into $(\frac{m-1}{M}, \frac{m}{M}]$ in M bins.

On the other hand, since $p(f(x); \alpha) \in (0, 1]$, we also have

$$\max_{y \in \mathcal{Y}} [\sigma(p(f(x); \alpha) * g(f(x)))]_y \leq \max_{y \in \mathcal{Y}} [\sigma(g(f(x)))]_y, \quad (51)$$

and this yields

$$\frac{1}{|B_m|} \sum_{i \in B_m} \max_{y \in \mathcal{Y}} [\sigma(p(f(x_i); \alpha) * g(f(x_i)))]_y \leq \frac{1}{|B_m|} \sum_{i \in B_m} \max_{y \in \mathcal{Y}} [\sigma(g(f(x_i)))]_y. \quad (52)$$

Furthermore, by assuming the predictive distribution of the standard softmax layer $\sigma(g(f(x)))$ is over-confident, i.e., $\text{acc}(B_m) \leq \text{conf}(B_m), \forall B_m$, then we have

$$0 \leq \frac{1}{|B_m|} \sum_{i \in B_m} \mathbb{I}(\arg \max_{y \in \mathcal{Y}} [\sigma(g(z_i))]_y = y_i) \leq \frac{1}{|B_m|} \sum_{i \in B_m} \max_{y \in \mathcal{Y}} [\sigma(g(z_i))]_y, \forall B_m. \quad (53)$$

Combining with the result in 49, in 52 and in 52 together, for N number of samples, we obtain

$$\sum_{m=1}^M \frac{|B_m|}{N} \left| \frac{1}{|B_m|} \sum_{i \in B_m} \mathbb{I}(\arg \max_{y \in \mathcal{Y}} [\sigma(p(z_i; \alpha) * g(z_i))]_y = y_i) - \frac{1}{|B_m|} \sum_{i \in B_m} \max_{y \in \mathcal{Y}} [\sigma(p(z_i; \alpha) * g(z_i))]_y \right| \quad (54)$$

$\underbrace{\hspace{15em}}_{\text{ECE}(\sigma((p(f; \alpha) * g) \circ f))}$

$$\leq \sum_{m=1}^M \frac{|B_m|}{N} \left| \frac{1}{|B_m|} \sum_{i \in B_m} \mathbb{I}(\arg \max_{y \in \mathcal{Y}} [\sigma(g(z_i))]_y = y_i) - \frac{1}{|B_m|} \sum_{i \in B_m} \max_{y \in \mathcal{Y}} [\sigma(g(z_i))]_y \right|, \text{ where } z_i = f(x_i). \quad (55)$$

$\underbrace{\hspace{15em}}_{\text{ECE}(\sigma(g \circ f))}$

As a consequence, we obtain the conclusion: $\text{ECE}(\sigma((p(f; \alpha) * g) \circ f)) \leq \text{ECE}(\sigma(g \circ f))$ of Proposition 5.7. \square

B Further discussion and Ablation study

This appendix will make a detailed discussion about our implementation to control the range of the likelihood value in Algorithm 1 and distance preserving assumption on latent space in Proposition 5.5.

B.1 Density estimation and likelihood value

Algorithm 2 Scaling likelihood

Scaling Input: Training data D_s , encoder f , trained density function $p(Z; \hat{\alpha})$.

$\text{max_trainNLL} \leftarrow 0$

for $e = 1 \rightarrow \text{epochs}$ **do**

Sample D_B with a mini-batch B for source data D_s

$Z = f(X \in D_B)$

$\text{batch_trainNLL} \leftarrow p(Z; \hat{\alpha})$

if $\text{max}(\text{batch_trainNLL}) > \text{max_trainNLL}$ **then**

$\text{max_trainNLL} \leftarrow \text{max}(\text{batch_trainNLL})$

end if

end for

Scaling Inference Input: Test sample x_t

$z_t = f(x_t)$

$p(z_t; \hat{\alpha}) = \frac{p(z_t; \hat{\alpha})}{\text{max_trainNLL}}$

Recall that the output in the inference step of Algorithm 1 has the form

$$p(y = i | x_t) = \frac{\exp(p(z_t; \hat{\alpha}) * (z_t^\top \theta_{g_i}))}{\sum_{j=1}^K \exp(p(z_t; \hat{\alpha}) * (z_t^\top \theta_{g_j}))}, \forall i \in \mathcal{Y}. \quad (56)$$

Let's consider: $\exp(p(z_t; \hat{\alpha}) * (z_t^\top \theta_{g_i}))$, if the likelihood value of $p(z_t; \hat{\alpha})$ is too large, then the output of the exponential function may go to a very large value, leading to the computer can not store to compute. Therefore, we need to find a scaling technique to avoid this issue.

Recall that for density estimation, we use KDE for the toy dataset and Normalizing-Flows Real-NVP [65, 66] for other datasets. Instead of returning likelihood value $p(Z; \hat{\alpha})$, both these estimations return the logarithm of likelihood $\log(p(Z; \hat{\alpha}))$, then we need to take exponentially to get the likelihood value by

$$p(Z; \hat{\alpha}) = e^{\log(p(Z; \hat{\alpha}))}. \quad (57)$$

By doing so, there will be two properties for the range of likelihood value $p(Z; \hat{\alpha})$. First, value of $p(Z; \hat{\alpha}) \neq 0$ by $\log(0)$ being undefined. Second, $p(Z; \hat{\alpha})$ is always positive by the output of the exponential function is always positive. As a result, we obtain the likelihood value $p(Z; \hat{\alpha})$ is in the range of $(0, +\infty]$.

To avoid the numerical issue when $p(Z; \hat{\alpha}) \rightarrow +\infty$, we use the scaling technique to scale the range $(0, +\infty]$ to $(0, 1]$ by the following formula

$$p(Z; \hat{\alpha}) = \frac{p(Z; \hat{\alpha})}{\max(p(Z_{train}; \hat{\alpha}))}. \quad (58)$$

It is also worth noticing that there also can be a case $e^{\log(p(Z; \hat{\alpha}))}$ in Equation 57 goes to $+\infty$ if $\log(p(Z; \hat{\alpha}))$ is too large, therefore, we also need to scale it to avoid the numerical issue. The pseudo-code of our scaling algorithm and inference process is presented in Algorithm 2.

B.2 Distance preserving on latent space

In order to make the feature extractor $f(x)$ satisfy distance preserving on latent space \mathcal{Z} in Definition 3.2, Liu et al. [11] has proposed adding Spectral-normalized layers into their framework to satisfy the bi-Lipschitz condition [77] as follows

$$L_1 * \|x_1 - x_2\|_{\mathcal{X}} \leq \|f(x_1) - f(x_2)\|_{\mathcal{Z}} \leq L_2 * \|x_1 - x_2\|_{\mathcal{X}}, \quad (59)$$

for positive and bounded constants $0 < L_1 < 1 < L_2$. Because the upper Lipschitz bound $\|f(x_1) - f(x_2)\|_{\mathcal{Z}} \leq L_2 * \|x_1 - x_2\|_{\mathcal{X}}$ prevents the hidden representation $f(x)$ from being overly sensitive to the semantically meaningless perturbations in the sample space \mathcal{X} . On the other hand, the lower Lipschitz bound $\|f(x_1) - f(x_2)\|_{\mathcal{Z}} \geq L_1 * \|x_1 - x_2\|_{\mathcal{X}}$ prevents the hidden representation $f(x)$ from being unnecessarily invariant to the semantically meaningful changes in the input manifold.

That said, we do not add Spectral-normalized layers into our framework for three reasons. First, adding Spectral-normalized layers will require a number of additional non-trainable parameters for storage, leading to unscalable across different modern DNN backbones (e.g., Figure 8 with Resnet-50 on ImageNet dataset). Second, to do Spectral Normalization for every weight in each residual layer, these non-trainable parameters will be computed with the power iteration method [31, 49], causing a high latency at inference time (see Figure 8). Finally, we find that those layers are actually unessential to make the predictive distribution to be distance aware in practice. As a result, in Proposition 5.5, we assume $f(x)$ satisfies distance preserving on latent space \mathcal{Z} .

Indeed, we next empirically show the Spectral-normalized layers are unessential if we do ERM in the first step of our Algorithm 1. Figure 7 compares the performance of SNGP and Density-Softmax with and without the Spectral-normalized layers. We observe that the performance of SNGP with and without Spectral-normalized layers is almost the same, and the Gaussian Process layer only is enough to make the model's prediction to be distance-aware. Similarly, in our Density-Softmax framework, adding Spectral-normalized layers are not necessary because we are doing ERM which also can help feature extractor $f(x)$ to be distance preserving on latent space \mathcal{Z} .

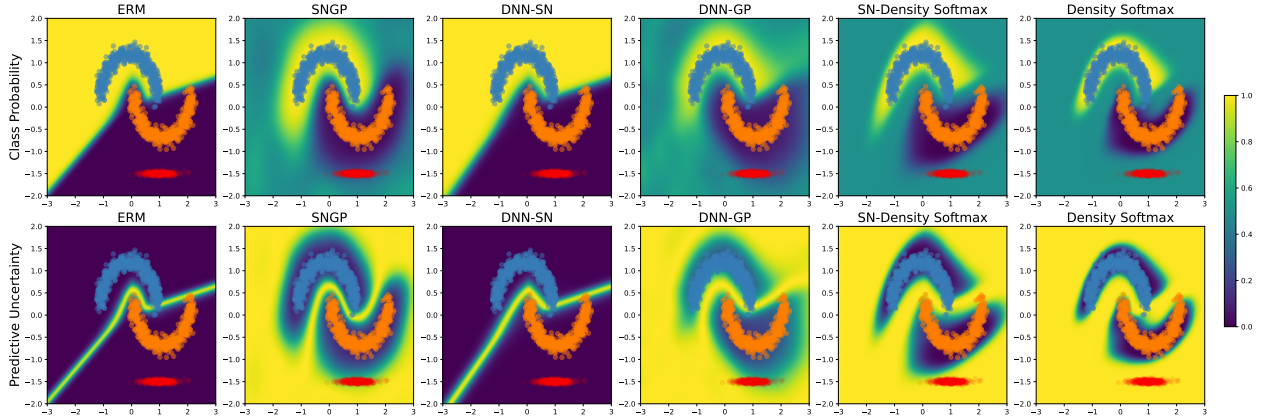


Figure 7: The class probability $p(y|x)$ (Top Row) and predictive uncertainty $var(y|x) = p(y|x) * (1 - p(y|x))$ surface (Bottom Row) with different estimation approaches. **The performance between with and without Spectral-normalized layers are almost the same in SNGP and Density-Softmax.**

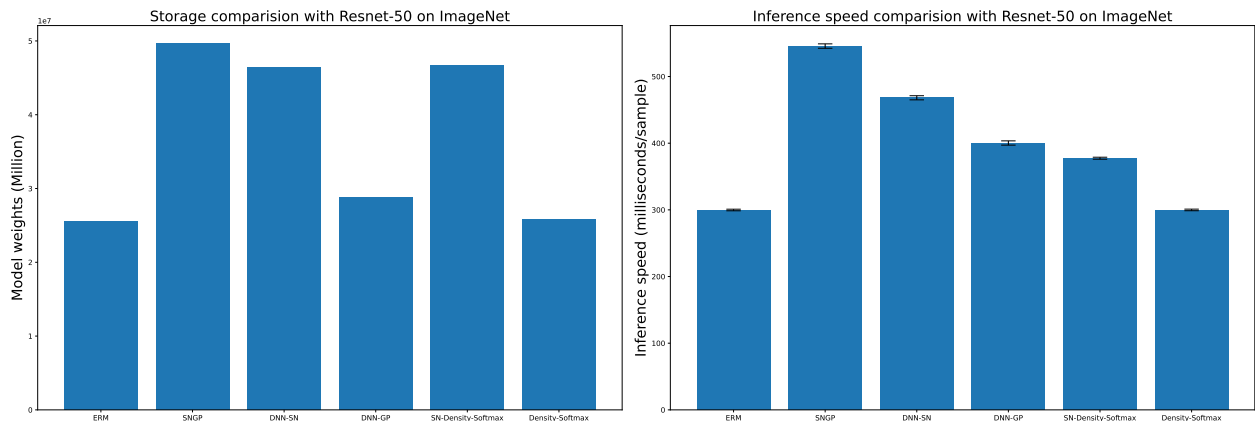


Figure 8: Comparison in model storage requirement (Million weights) and inference speed (milliseconds per sample) with error bars across 10 seeds of Resnet-50 on ImageNet dataset. **Adding Spectral Normalization or Gaussian Process layers causes the high number of model weights and latency.**

C Additional experiments

C.1 Dataset details

This appendix provides more detail about the datasets used in our experiments. Figure 10 visualizes examples for the vision and language benchmark datasets. There are total of 7 datasets (containing the toy dataset in Figure 9) widely used for classification tasks in distributional shifts, including:

- **Toy dataset [11]** includes two types of 2D classification datasets—two moons and two ovals. For the training dataset which is represented by the two in-domain classes (500 orange and 500 blue data points), the two moons consist of two banana-shaped distributions separable by nonlinear decision boundary. In contrast, the two ovals consist of two near-flat Gaussian distributions that are separable by a linear decision boundary. For the OOD set, we generate and color by 500 red data points.
- **CIFAR-10-C [68]** contains 10,000 colored samples of dimension $(3, 32, 32)$ with 10 classes in classification problem. The distributional shifts data are generated from the test images of CIFAR-10 [78] over a total of 15 corruptions, with 15 standard noise type $d \in \{\text{identity, gaussian noise, shot noise, impulse noise, defocus blur, frosted glass blur, motion blur, zoom blur, snow, frost, fog, brightness, contrast, elastic, pixelate, jpeg compression}\}$. For each noise corruption, there are 5 skew intensities represented for the level noise to evaluate the robustness, so we have a total of 75 OOD test sets.

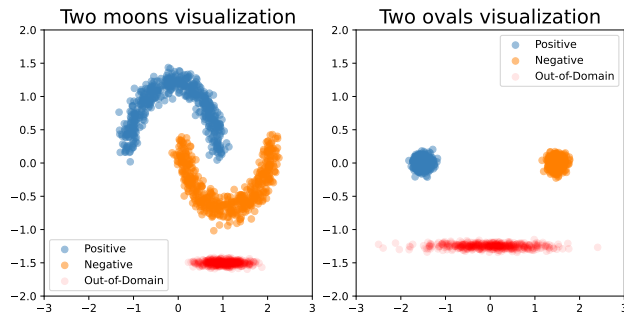


Figure 9: Data visualization on the Toy dataset with two moons (Left) and two ovals (Right) 2D classification. Training data for positive (Orange) and negative classes (Blue). OOD data (Red) are not observed during training.

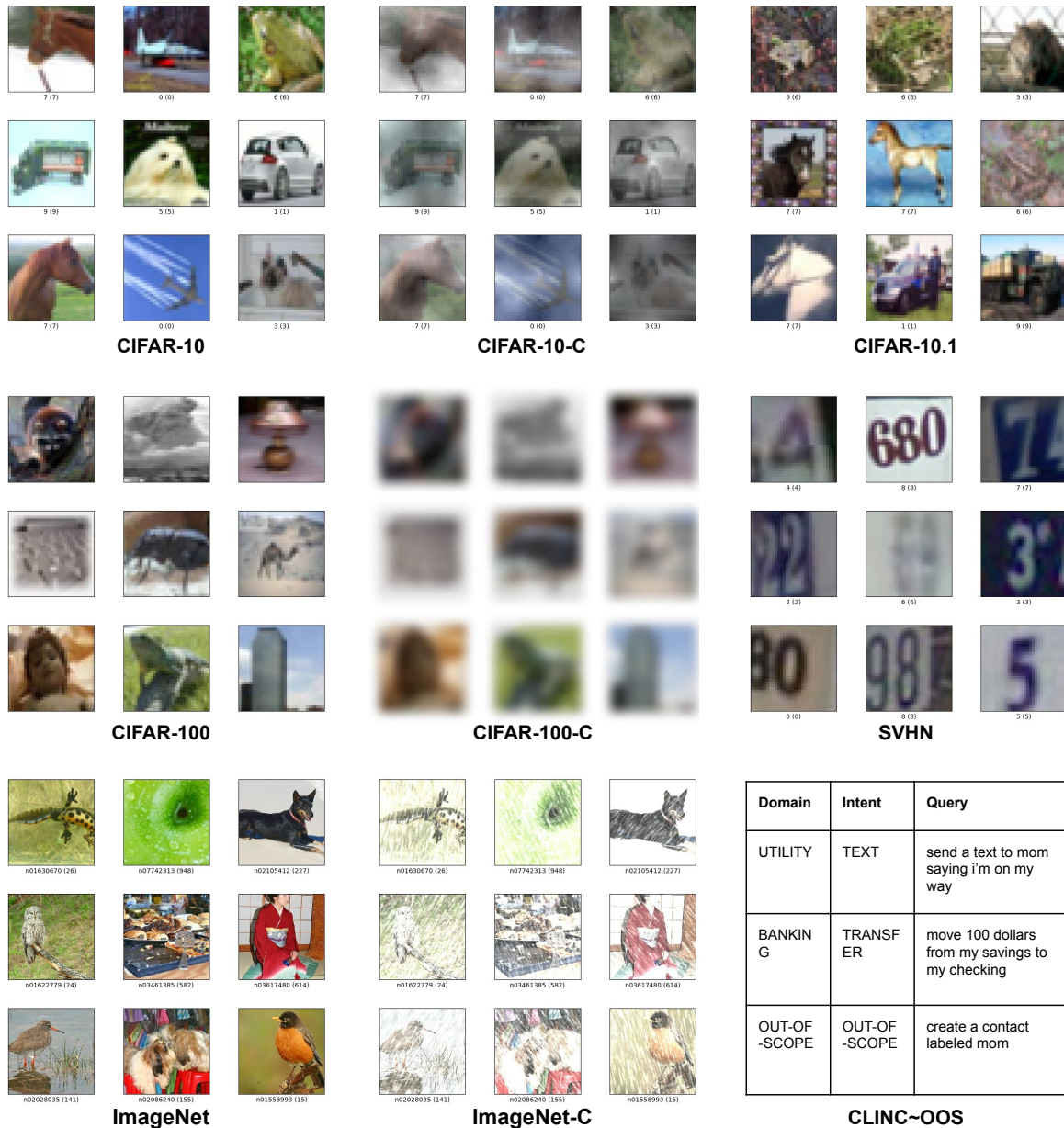


Figure 10: The benchmark dataset summarizations. For each dataset, we pick random images and show corresponding shifted images from random distributional shifts set. For CIFAR-10-C is fog_5, CIFAR-100-C is blurring, and ImageNet-C is snow_5. CIFAR-10.1 is the real-world distributional shift.

- **CIFAR-10.1** [70] has 2,021 images for version v4 and 2,000 images with class balanced for version v6, of dimension (3, 32, 32) in classification problem with the same 10 classes in CIFAR-10. The dataset is

collated in real-world images on the Internet and is a subset of the Tiny Images [79]. This is used to additionally test the reliability of models under real-world distributional shifts.

- **CIFAR-100-C [68]** has 100 classes containing 100 testing images of dimension (3, 32, 32) per each class. The distributional shifts are generated from the CIFAR-100 [78] test set over a total of 17 corruptions, with 17 noise type $d \in \{\text{identity, gaussian noise, shot noise, impulse noise, defocus blur, gaussian blur, motion blur, zoom blur, frost, fog, brightness, contrast, elastic transform, pixelate, jpeg compression, saturate, spatter, speckle noise}\}$. Similar to CIFAR-10-C, there are 5 skew intensities for each noise corruption, as a result, we have a total of 85 OOD test sets.
- **SVHN [69]** contains 600,000 digit images coming from real-world data of dimension (3, 32, 32). We use this as a far domain to test OOD detection performance with CIFAR.
- **ImageNet-C [68]** includes 50,000 photos of dimension (3, 224, 224) in classification problem with 1000 object categories, generated from the test images of ImageNet [80] with corruptions and skew intensities similar to CIFAR-10-C. Therefore, we also have a total of 75 OOD test sets.
- **CLINC OOS [71]** covers 150 intent classes over 10 IID domain services with 150 training query sentences in each domain, and 1500 natural OOD utterances. We use this natural language dataset as a realistic benchmarking text classification in task-driven dialog systems.

C.2 Baseline details

This appendix provides an exhaustive literature review of 13 SOTA related methods which are used to make comparisons with our model:

- **ERM [21]** is a standard deterministic model. In inference time, it predicts the label immediately by a single forward pass.
- **MC Dropout [12]** includes dropout regularization method in the model. In inference time, it uses MC sampling by dropout to make different predictions, then get the mean of the list prediction.
- **MFVI BNN [15, 16]** uses the BNN Network by putting distribution over the weight by mean and variance per each weight. In inference time, it samples weight distribution by MC to make different predictions, then gets the mean of the list prediction. Because each weight consists of mean and variance, the total model weights will double as the ERM model.
- **Rank-1 BNN [18]** uses the mixture approximate posterior to benefits from multimodal representation with local uncertainty around each mode, compute posterior on rank-1 matrix while keeping weight is deterministic. In inference time, it samples weight distribution by MC to make different predictions, then gets the mean of the list prediction.
- **ENN [43]** makes use of conjugate prior property in Bayesian Inference to compute Dirichlet distribution on class probabilities in closed-form. Although this method can improve computational efficiency at inference time, it is sensitive to hyper-parameters by selecting Prior’s parameters, leading to poor results in uncertainty and robustness performance in benchmarking (see Table 3).
- **Posterior Net [24]** is a combination of ENN with a latent density function by utilized conditional densities per class, intuitively acting as class conditionals on the latent space. Due to belonging to the Bayesian perspective, this framework also needs to select a "good" Prior distribution, which is often difficult in practice.
- **DUQ [22]** is a deterministic-based framework by using kernel distance with Radial Basis Function (RBF) to improve OOD detection ability. However, it has been shown often to have a poor performance in uncertainty and robustness [5, 11]. Regarding scalability, this requires storing and computing a weight matrix with the size depending quadratically on latent dimension and linearly in the number of classes, leading to high computational demands across modern DNN architectures at inference time.

- **DDU [23, 40]** is another deterministic-based method, which is a combination of ERM with a Gaussian Mixture Models (GMM) density function to detect OOD samples. However, this OOD detector does not contribute to the predictive distribution of the softmax directly. As a result, this method needs to apply the post-hoc re-calibration technique to improve calibration performance. Additionally, it also requires storing a covariance matrix in GMM function with the same size as the weight matrix in DUQ, leading to limiting the scalability at inference time.
- **NUQ [38]** is also a combination of a deterministic-based approach with density function. However, similar to DDU, the density function does not directly contribute to the predictive distribution with KNN, leading to poor performance in terms of calibrated uncertainty. This framework also suffers from computational issues because it is a non-parametric model, which needs to store and compare with training data points at inference time.
- **DNN-GP [10, 11]** replaces the Dense output layer of DNN with a Gaussian process layer to produce predictive distribution. In inference time, it uses MC sampling to calculate closed-form predictive distribution posterior mean to make different predictions, then get the mean of the list prediction.
- **SNGP [11]** is a combination of DNN-GP with Spectral Normalization to the hidden layers. Because using the Spectral Normalization for every weight in each residual layer with the power iteration method [31, 49], and Gaussian Process layer with MC sampling, the weight and latency of SNGP is considerably higher than the ERM model at inference time.
- **BatchEnsemble [32]** defines each weight matrix to be the Hadamard product of a shared weight among all ensemble members and a rank-one matrix per member. In inference time, the final prediction is calculated from the mean of the list prediction of the ensemble.
- **Deep Ensembles [19, 20]** includes multiple deterministic model trained with different seeds. In inference time, the final prediction is calculated from the mean of the list prediction of the ensemble. Due to aggregates from multiple deterministic models, the total of model weights need to store will increase linearly w.r.t. the number of models.

C.3 Implementation details

In this appendix, we describe the data-processing techniques, neural network architectures, hyper-parameters, and details for reproducing our experiments. Based on the code of Nado et al. [5], we use similar settings with them for everything for a fair comparison on the benchmark dataset. For the setting on the toy and CLINC OOS dataset, we follow the settings of Liu et al. [11].

Data processing techniques. We only use normalization to process images for the benchmark datasets. Specifically, for CIFAR-10 and CIFAR-100, we normalize by the mean is [0.4914, 0.4822, 0.4465] and standard deviation is [0.2470, 0.2435, 0.2616]. For ImageNet, we normalize by the mean is [0.485, 0.456, 0.406] and standard deviation is [0.229, 0.224, 0.225] (note that we do not perform augmentation techniques of Hendrycks* et al. [81]). For CLINC OOS, we apply BERT pre-tokenizer [74] to the sentences with maximum sequence length 32 with binary input mask that returns 1 for valid tokens.

Architectures and hyper-parameters. We list the detailed value of hyper-parameters used for each dataset in Table 1. For a fair comparison with deterministic, we always use the exact same hyper-parameters as the Deterministic-ERM. Depending on the dimensions of latent variable Z in space $\mathcal{Z} \subset \mathbb{R}^{d_z}$ for each backbone, we use different density estimation techniques. Specifically, for the toy dataset with the backbone is ResFFN-12-128 [11], we use KDE to estimate the density of $Z \in \mathbb{R}^{128}$. For higher dimensions with $Z \in \mathbb{R}^{640}$ in Wide Resnet-28-10 [72] on CIFAR-10-100, $Z \in \mathbb{R}^{768}$ in BERT [74] on CLINC OOS, and $Z \in \mathbb{R}^{2048}$ in Resnet-50 [73] on ImageNet, we use Normalizing-Flows Real-NVP [65, 66] which has the two Coupling structure in Table 2.

Dataset, source code, and computing system. The source code is provided in the mentioned GitHub in the main paper, including our notebook demo on the toy dataset, scripts to download the benchmark dataset, setup for environment configuration, and our provided code (detail in README.md). We run the code on two single GPUs: NVIDIA RTX A5000-24564MiB with 8 CPUs: AMD Ryzen Threadripper 3960X 24-Core, RAM: 64GB, and require 100GB available disk space for storage.

Table 1: Condition dataset, hyper-parameters, and their default values in our experiments. Settings are inherited from Liu et al. [11] for the toy dataset and from Nado et al. [5] for CIFAR-10-100 and ImageNet. **Note that we always use the exact same hyper-parameters as the Deterministic-ERM for a fair comparison.**

Conditions	Hyper-parameters	Default value
Toy dataset	backbone	ResFFN-12-128 [11]
	epochs	100
	batch size	128
	optimizer	Adam [82]
	learning rate	1e-4
	density estimation (KDE)	KDE(kernel = 'gaussian')
	density estimation epochs (Flows)	3000
	density optimizer (Flows)	Adam [82]
	density learning rate (Flows)	1e-4
	CIFAR-10-100	backbone
epochs		200
checkpoint interval		25
batch size		64
optimizer		SGD(momentum = 0.9, nesterov = True)
learning rate		0.05
lr decay epochs		[60, 120, 160]
lr decay ratio		0.2
L2 regularization coefficient		2e-4
scale range		-[0.55-0.4, 0.4-0.3]
density estimation epochs		50
density optimizer		Adam [82]
density learning rate		1e-4
re-optimize classifier epochs		10
ImageNet		backbone
	epochs	90
	checkpoint interval	25
	batch size	64
	optimizer	SGD(momentum = 0.9, nesterov = True)
	learning rate	0.05
	lr decay epochs	[30, 60, 80]
	lr decay ratio	0.1
	L2 regularization coefficient	1e-4
	scale range	-[0.4, 0.3]
	density estimation epochs	10
	density optimizer	Adam [82]
	density learning rate	1e-4
	re-optimize classifier epochs	2
	CLINC OOS	backbone
epochs		150
checkpoint interval		5
batch size		64
optimizer		Adam [82](momentum = 0.9)
learning rate		1e-4
L2 regularization coefficient		1e-4
density estimation epochs		10
density optimizer		Adam [82]
density learning rate		1e-4
re-optimize classifier epochs		2

Table 2: Two Coupling structures-(a) and (b) for Normalizing-Flows Real-NVP [65, 66] on CIFAR-10, CIFAR-100, ImageNet, and CLINC OOS. Input: $Z \in \mathbb{R}^{d_z}$, where $d_z = 640$ for Wide Resnet-28-10 [72], $d_z = 768$ for BERT [74], and $d_z = 2048$ for Resnet-50 [73]

(a) S_{θ_s}	(b) T_{θ_r}
Input: $Z \in \mathbb{R}^{d_z}$	Input: $Z \in \mathbb{R}^{d_z}$
Dense (units = 16, regularizers l2 = 0.01, ReLU)	Dense (units = 16, regularizers l2 = 0.01, ReLU)
Dense (units = 16, regularizers l2 = 0.01, ReLU)	Dense (units = 16, regularizers l2 = 0.01, ReLU)
Dense (units = 16, regularizers l2 = 0.01, ReLU)	Dense (units = 16, regularizers l2 = 0.01, ReLU)
Dense (units = 16, regularizers l2 = 0.01, ReLU)	Dense (units = 16, regularizers l2 = 0.01, ReLU)
Dense (units = 16, regularizers l2 = 0.01, Tanh)	Dense (units = 16, regularizers l2 = 0.01, Linear)

C.4 Empirical result details

In this appendix, we provide additional results from the experiments, including distance-aware visualizations on the toy dataset, detailed results for distributional shifts comparison between methods, calibration uncertainty, and predictive entropy on the benchmark datasets.

C.4.1 Distance awareness on the toy dataset

In the main paper, we have shown Density-Softmax is a distance-aware method on two moons dataset with the variance of Bernoulli distribution surface. In order to test whether this observation is consistent across different settings, we continue to do experiments with different uncertainty metrics and datasets. It is also worth noticing that we have used KDE on the toy dataset to estimate latent representation $Z \in \mathbb{R}^{128}$ from the ResFFN-12-128 [11] backbone. However, we also can use different density estimation techniques. Therefore, to test our method behavior with different estimation approaches, we do an ablation study with three additional settings, including using KDE on sample space $\mathcal{X} \subset \mathbb{R}^2$ instead of \mathcal{Z} , and replacing KDE by Normalizing Flows and also estimating on both sample space \mathcal{X} and latent space \mathcal{Z} .

Different uncertainty metrics. Figure 11 presents a comparison in terms of predictive entropy which have the following formula

$$H(Y|X = x) = -p(y|x) * \log_2(p(y|x)) - (1 - p(y|x)) * \log_2((1 - p(y|x))). \quad (60)$$

Because of the over-confidence of deterministic-ERM, MC Dropout, Rank-1 BNN, and Ensemble which return $p(y|x) = 0$, their predictive entropy become undefined by $\log_2(p(y|x)) = \log_2(0)$ is undefined. As a result, we have a white background for these mentioned baselines, showing these methods are not able to be aware of the distance OOD dataset. For MC Dropout and Ensemble, since these two methods do not provide a convenient expression of the predictive variance of Bernoulli distribution, we also follow the work of Liu et al. [11] to plot their predictive uncertainty as the distance of the maximum predictive probability from 0.5, i.e.,

$$u(x) = 1 - 2 * |p(y|x) - 0.5|, \quad (61)$$

so that $u(x) \in [0, 1]$ in Figure 12. Although with different uncertainty metrics, deterministic-ERM, MC Dropout, Rank-1 BNN, and Ensemble still perform badly, showing truly unable to have the distance-aware ability. Meanwhile, compare with SNGP, our Density-Softmax performance is still better with 1.0 values on both uncertainty surfaces in these two figures while SNGP still make significant mistakes with low uncertainty value on OOD data.

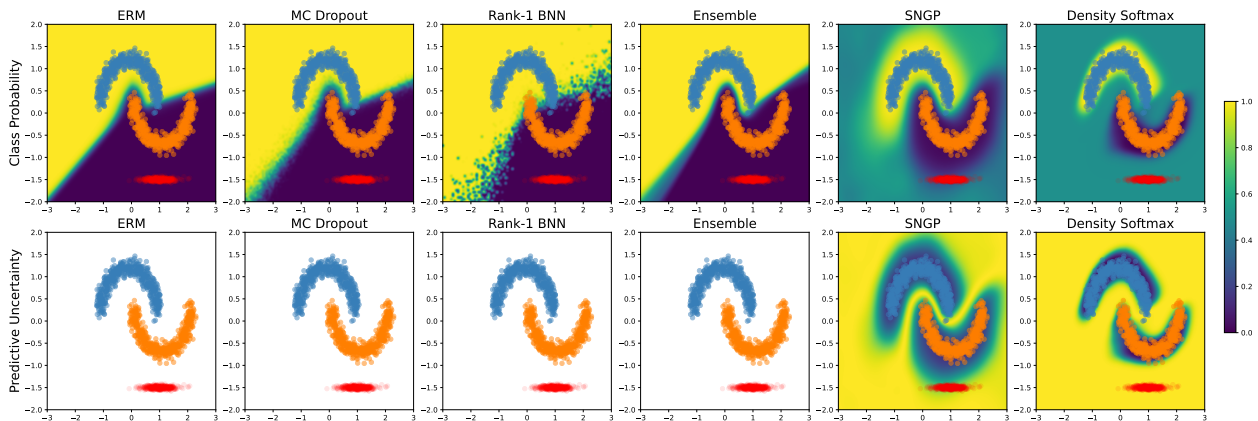


Figure 11: The class probability $p(y|x)$ (Top Row) and predictive entropy $H(Y|X = x) = -p(y|x) * \log_2(p(y|x)) - (1 - p(y|x)) * \log_2((1 - p(y|x)))$ surface (Bottom Row) of our Density-Softmax versus different approaches. **Our Density-Softmax achieves distance awareness with a uniform class probability and high entropy value on OOD data.** Note that the white background due to $\log(0)$ is undefined.

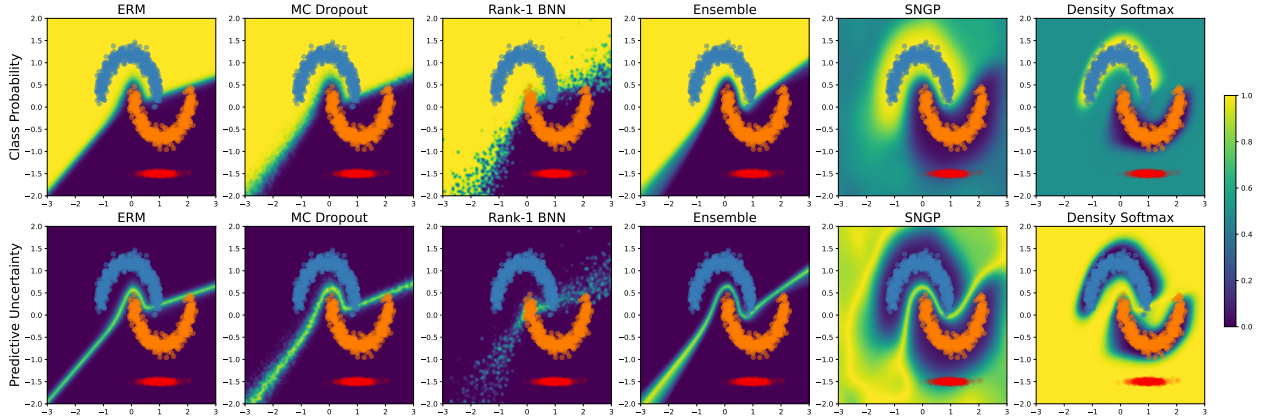


Figure 12: The class probability $p(y|x)$ (Top Row) and predictive uncertainty $u(x) = 1 - 2 * |p(y|x) - 0.5|$ surface (Bottom Row) of our Density-Softmax versus different approaches. **Our Density-Softmax achieves distance awareness with a uniform class probability and high uncertainty value on OOD data.**

Different toy dataset. To continue to verify a consistency observation across different empirical settings, we illustrate distance-aware ability by predictive variance surface on the second toy dataset. Figure 13 compares the methods as mentioned earlier on two ovals datasets. Similar to previous settings, only SNGP is able to show its distance-aware uncertainty. However, for around half of OOD data points, its predictive uncertainty is still 0.0, showing still has limitations in distance-aware ability. In contrast, our Density-Softmax performs well, with 0.0 uncertainty value on IID training data points while always returning 1.0 on OOD data points, continue confirming the hypothesis that our Density-Softmax is a better distance-aware method.

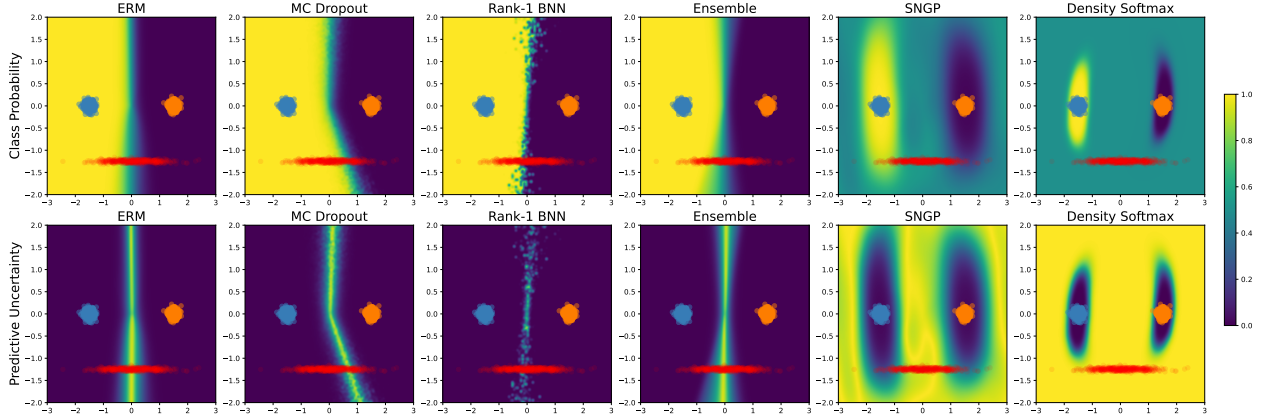


Figure 13: The class probability $p(y|x)$ (Top Row) and predictive uncertainty $u(x) = 1 - 2 * |p(y|x) - 0.5|$ surface (Bottom Row) of our Density-Softmax versus different approaches on the two ovals 2D classification benchmarks. Training data for positive (Orange) and negative classes (Blue). OOD data (Red) are not observed during training. Background color represents the estimated model's class probability and predictive uncertainty. **Our Density-Softmax achieves distance awareness with a uniform class probability and high uncertainty value on OOD data.**

Different density estimations. Recall that we use KDE on latent space $\mathcal{Z} \subset \mathbb{R}^{128}$ with the ResFFN-12-128 [11] backbone for the toy dataset. Rather, we can use a much simple estimation on sample space $\mathcal{X} \subset \mathbb{R}^2$ on this 2D dimension dataset. Moreover, we also can use Normalizing-Flows Real-NVP [65, 66] to replace KDE to make the estimation algorithm consistent across different experimental settings. Therefore, we provide these mentioned estimation settings in Figure 14. It can be seen that there are no differences between the estimation on latent space \mathcal{Z} and sample space \mathcal{X} . Meanwhile, there is a minor difference between

KDE and Normalizing-Flows with a slight degradation performance in Normalizing-Flows estimation. As a result, we select the estimation on latent space \mathcal{Z} to consistency with our Algorithm 1 while using KDE to show our best performance.

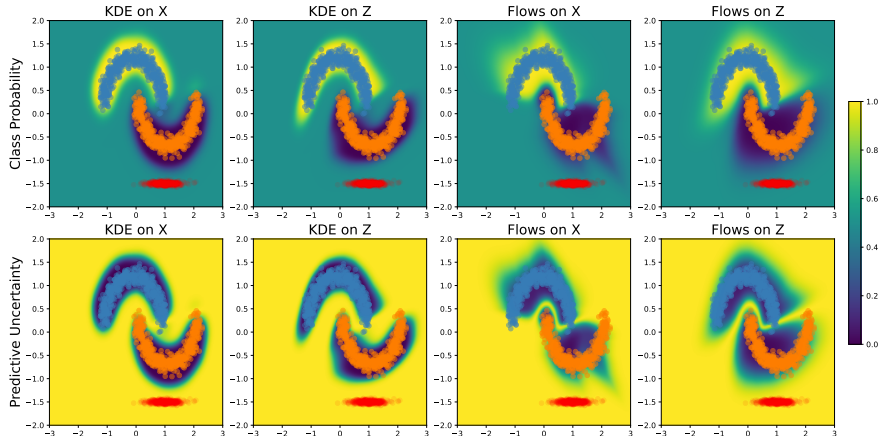


Figure 14: The class probability $p(y|x)$ (Top Row) and predictive uncertainty $var(y|x) = p(y|x) * (1 - p(y|x))$ surface (Bottom Row) with different estimation approaches. KDE directly on sample space $\mathcal{X} \subset \mathbb{R}^2$ (Left) and on latent space $\mathcal{Z} \subset \mathbb{R}^{128}$ (Middle-Left). Normalizing-Flows Real-NVP [65, 66] on sample space $\mathcal{X} \subset \mathbb{R}^2$ (Middle-Right) and on latent space $\mathcal{Z} \subset \mathbb{R}^{128}$ (Right).

C.4.2 Benchmark result details

Table 3, 4, 5, and 6 are detailed results for each dataset which we deferred from the main paper. In particular, Table 3 is the result of Wide Resnet-28-10, which is trained on CIFAR-10, and tested on CIFAR-10 for IID, CIFAR-10-C, CIFAR-10.1 for OOD, SVHN, and CIFAR-100 for OOD detection. Table 4 is the result of Wide Resnet-28-10, which is trained on CIFAR-100 and tested on CIFAR-100 for IID, CIFAR-100-C for OOD, SVHN, and CIFAR-10 for OOD detection. Table 5 is the result of Resnet-50, which is trained on Imagenet, tested on Imagenet for IID, and Imagenet-C for OOD. Table 6 is the result of BERT, which is trained and tested on CLINC OOS for IID and OOD detection. Figure 4 in the main paper is the summarizing of these tables per each criterion. Specifically, for each sub-figure in Figure 4, the x-axis represents the model’s weight (#Params), the y-axis represents the inference time (Latency), and the z-axis is the mean (average) for each criterion. For instance, in Figure 4, the z-axis in the first sub-figure of NLL with CIFAR-10 will be computed by the mean of the NLL, the cNLL, and the oNLL columns from Table 3. The main observations, analyses, and conclusions from this Figure and Tables are provided in Section 6 of the main paper.

In order to compare the robustness between methods from the above results, we visualize Figure 15, the box plots of the NLL, accuracy, and ECE across corruptions under distributional shifts level in CIFAR-100 based dataset from Table 4. Overall, besides achieving the lowest NLL and ECE in average, our Density-Softmax also always achieves the best NLL and ECE performance across different shift intensities in Figure 15. For each intensity, our results also show a low variance, implying the stability of our algorithm across different corruption types. *More importantly, compared to the second-best method Rank-1 BNN, the gap between our two methods increases when the level shift increases, showing our Density-Softmax is more robust than theirs under distributional shifts.*

Figure 15 however only shows the statistics across different shift methods. Therefore, we next analyze in detail the above results over 10 different random seeds. Specifically, we train each model with a specific random seed, then evaluate the result. We repeatedly do this evaluation 10 times with 10 different seed values. Finally, collect 10 of these results together and visualize the mean and standard deviation by the error bar for each shift intensity level. *Figure 16 shows these results in the CIFAR-10-C setting from Table 3, we observe that the result of our model and other baselines have a small variance, showing the consistency and stability across different random seeds.*

Table 3: Results for Wide Resnet-28-10 on CIFAR-10, averaged over 10 seeds: negative log-likelihood (lower is better), accuracy (higher is better), and expected calibration error (lower is better). NLL, Acc, and ECE are represented for performance on IID test set. cNLL, cAcc, and cECE are NLL, accuracy, and ECE averaged over CIFAR-10-C’s corruption types & intensities while oNLL, oAcc, and oECE are for real-world distribution shift over CIFAR-10.1. AUPR-S and AUPR-C are AUPR for OOD detection on SVHN and CIFAR-100 (higher are better). #Params is the number of model parameters while Latency is the milliseconds to inference per sample, and are colored by blue in our method (lower are better). Best scores with the significant test are marked in **bold**.

Method	NLL(↓)	Acc(↑)	ECE(↓)	cNLL(↓)	cAcc(↑)	cECE(↓)	oNLL(↓)	oAcc(↑)	oECE(↓)	AUPR-S(↑)	AUPR-C(↑)	#Params(↓)	Latency(↓)
CIFAR-10 & CIFAR-10-C & CIFAR-10.1													
ERM	0.159	96.0	0.023	1.05	76.1	0.153	0.40	89.9	0.064	0.781	0.835	36.50M	518.12
MC Dropout	0.148	95.9	0.020	1.05	75.6	0.150	0.39	89.9	0.058	0.971	0.832	36.50M	1,551.34
MFVI BNN	0.208	95.0	0.027	1.58	71.0	0.183	0.49	88.1	0.070	0.780	0.828	72.96M	2,564.58
Rank-1 BNN	0.128	96.3	0.008	0.84	76.7	0.080	0.32	90.4	0.033	0.963	0.885	36.65M	2,388.08
ENN	0.288	91.5	0.071	1.10	73.4	0.149	0.43	87.6	0.062	0.784	0.830	36.51M	958.59
Posterior Net	0.360	93.1	0.112	1.06	75.2	0.139	0.42	87.9	0.053	0.893	0.812	36.51M	1,162.48
DUQ	0.239	94.7	0.034	1.35	71.6	0.183	0.49	87.9	0.068	0.973	0.854	40.61M	1,538.35
DDU	0.159	96.0	0.024	1.06	76.0	0.153	0.39	89.8	0.063	0.986	0.887	40.61M	1,354.31
NUQ	0.301	92.0	0.106	1.72	73.2	0.188	0.50	87.6	0.068	0.702	0.810	68.50M	1,614.67
DNN-GP	0.221	95.9	0.029	1.38	71.7	0.175	0.56	89.8	0.081	0.976	0.887	39.25M	988.94
SNGP	0.138	95.9	0.018	0.86	75.6	0.090	0.43	89.7	0.064	0.990	0.905	44.39M	1,107.68
BatchEnsemble	0.136	96.3	0.018	0.97	77.8	0.124	0.35	90.6	0.048	0.897	0.801	36.58M	1,498.01
Deep Ensembles	0.114	96.6	0.010	0.81	77.9	0.087	0.28	92.2	0.025	0.964	0.888	145.99M	1,520.34
Density-Softmax	0.140	96.2	0.015	0.79	77.0	0.086	0.33	90.2	0.015	0.972	0.890	36.58M	520.53

Table 4: Results for Wide Resnet-28-10 on CIFAR-100: cNLL, cAcc, and cECE are for CIFAR-100-C. AUPR-S and AUPR-C are for SVHN and CIFAR-10.

Method	NLL(↓)	Acc(↑)	ECE(↓)	cNLL(↓)	cAcc(↑)	cECE(↓)	AUPR-S(↑)	AUPR-C(↑)	#Params(↓)	Latency(↓)
ERM	0.875	79.8	0.085	2.70	51.3	0.239	0.882	0.745	36.55M	521.15
MC Dropout	0.797	79.6	0.050	2.43	51.5	0.188	0.832	0.757	36.55M	1,562.39
MFVI BNN	0.933	77.3	0.094	3.15	48.0	0.283	0.882	0.748	73.07M	2,588.58
Rank-1 BNN	0.692	81.3	0.018	2.24	53.8	0.117	0.884	0.797	36.71M	2,402.04
Posterior Net	2.021	77.3	0.391	3.12	48.3	0.281	0.880	0.760	36.56M	1,190.87
DUQ	0.980	78.5	0.119	2.84	50.4	0.281	0.878	0.732	77.58M	1,547.35
DDU	0.877	79.7	0.086	2.70	51.3	0.240	0.890	0.797	77.58M	1,359.25
DNN-GP	0.885	79.2	0.064	2.63	47.7	0.166	0.876	0.746	39.35M	997.42
SNGP	0.847	79.9	0.025	2.53	50.0	0.117	0.923	0.801	44.48M	1,141.17
BatchEnsemble	0.690	81.9	0.027	2.56	51.3	0.149	0.870	0.757	36.63M	1,568.77
Deep Ensembles	0.666	82.7	0.021	2.27	54.1	0.138	0.888	0.780	146.22M	1,569.23
Density-Softmax	0.780	81.2	0.038	2.20	52.4	0.102	0.894	0.801	36.64M	522.94

Table 5: Results for Resnet-50 on ImageNet: cNLL, cAcc, and cECE are for ImageNet-C.

Method	NLL(↓)	Acc(↑)	ECE(↓)	cNLL(↓)	cAcc(↑)	cECE(↓)	#Params(↓)	Latency(↓)
ERM	0.939	76.2	0.032	3.21	40.5	0.103	25.61M	299.81
Rank-1 BNN	0.886	77.3	0.017	2.95	42.9	0.054	26.35M	1,383.65
SNGP	0.932	76.1	0.015	3.03	41.1	0.047	49.60M	545.70
BatchEnsemble	0.922	76.8	0.037	3.09	41.9	0.089	25.82M	696.81
Deep Ensembles	0.857	77.9	0.017	2.82	44.9	0.047	102.44M	701.34
Density-Softmax	0.950	76.3	0.024	2.99	41.0	0.050	25.88M	299.90

Table 6: Results for BERT on CLINC OOS.

Method	NLL(↓)	Acc(↑)	ECE(↓)	AUROC(↑)	AUPR(↑)	#Params(↓)	Latency(↓)
ERM	3.559	96.5	0.024	0.897	0.757	108.43M	1,071.88
MC Dropout	1.658	96.1	0.021	0.938	0.799	108.43M	3,880.63
DUQ	4.015	96.0	0.059	0.917	0.806	197.02M	1,296.12
DNN-GP	3.594	95.9	0.075	0.941	0.831	112.07M	1,279.91
SNGP	1.218	96.6	0.014	0.969	0.880	118.70M	1,485.95
Deep Ensembles	1.062	97.5	0.013	0.964	0.862	433.72M	3,875.74
Density-Softmax	1.552	96.5	0.019	0.938	0.840	108.53M	1,087.49

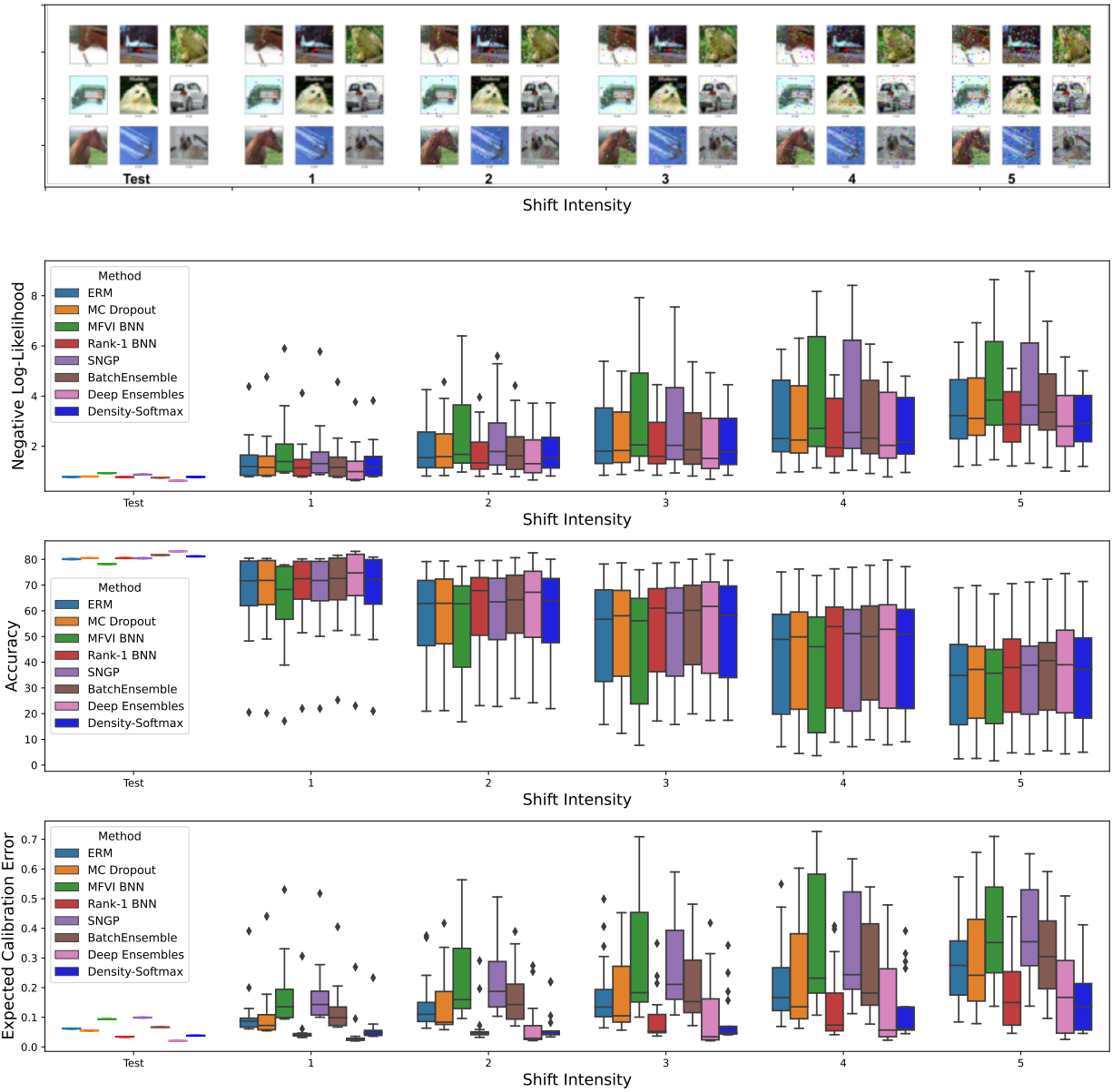


Figure 15: A corruption example by shift intensities and comparison under the distributional shift of negative log-likelihood, accuracy, and ECE under all types of corruptions in CIFAR-100-C. For each method, we show the mean on the test set and summarize the results on each shift intensity with a box plot. Each box shows the quartiles summarizing the results across all 17 types of shift while the error bars indicate the min and max across different shift types. **Our Density-Softmax achieves the lowest NLL and ECE with a low variance across different shift intensities.**

Similarly, Figure 17 is the comparison across 10 running with 10 different random seeds in terms of model storage and inference speed from Table 3. There is no variance in storage comparison since the model size is fixed and not affected by a random seed. Meanwhile, the latency variances across different seeds are minor since narrow error bars are in the inference speed comparison bar chart. *And this once again, confirms that the results are consistent and stable, our Density-Softmax is the fastest model with almost similar latency to a single Deterministic ERM.*

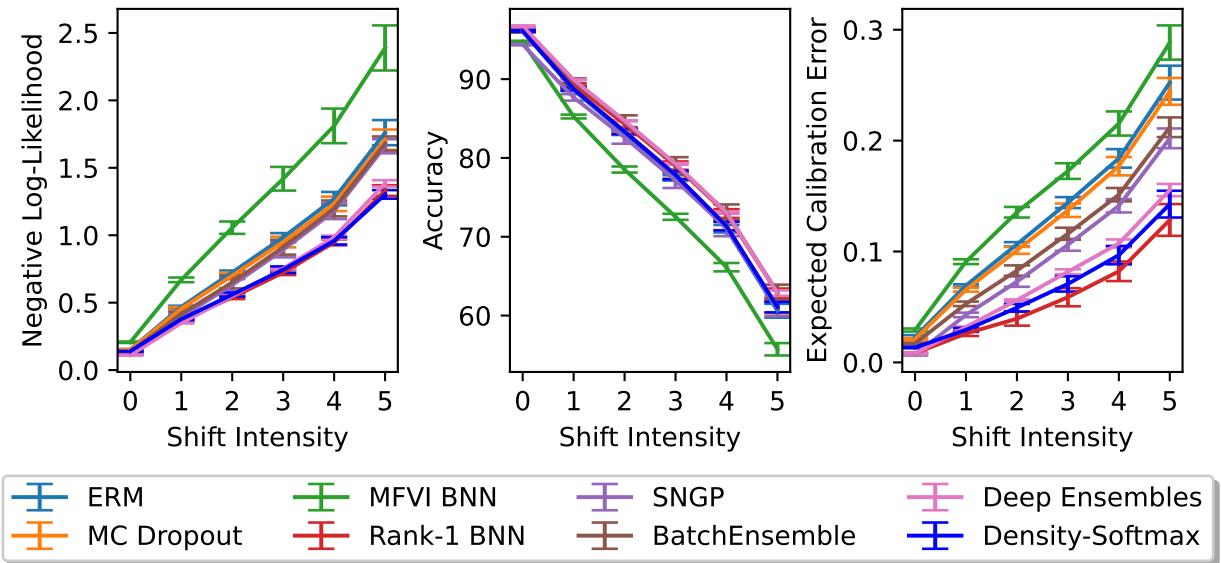


Figure 16: Benchmark performance in CIFAR-10-C with Wide Resnet-28-10 over 10 different random seeds. We plot NLL, accuracy, and ECE for varying corruption intensities; each result is the mean performance over 10 runs and 15 corruption types. The error bars represent a fraction of the standard deviation across corruption types. **Our method achieves competitive results with SOTA with low variance across different shift intensities.**

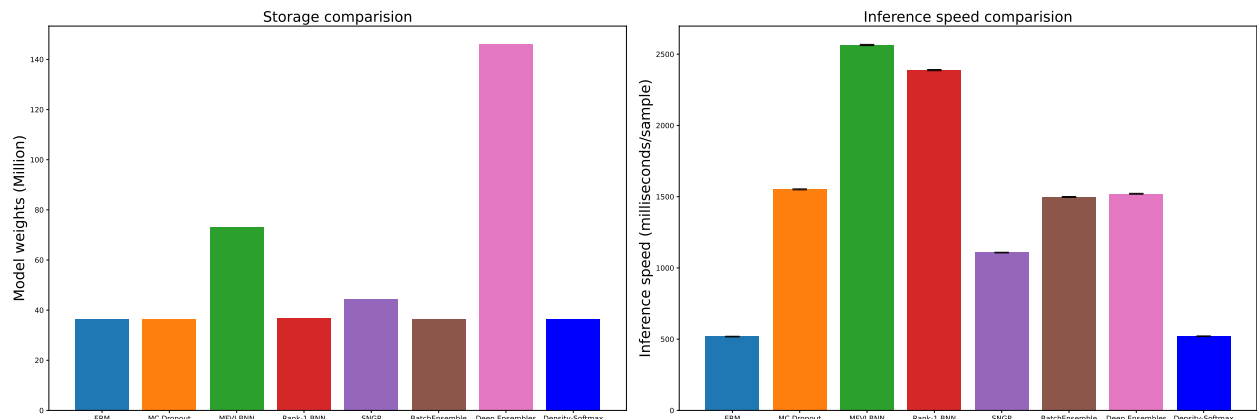


Figure 17: Comparison in model storage requirement (Million weights) and inference speed (milliseconds per sample) with error bars across 10 seeds of Wide Resnet-28-10 and CIFAR-10 dataset. **Our Density-Softmax achieves almost the same weight and inference speed with a single Deterministic ERM model, as a result, outperforming other baselines in computational efficiency.**

C.4.3 Calibration details.

To understand how models calibrate in more detail, we visualize the reliability diagrams to test the model’s confidence across IID and OOD settings. For IID setting in CIFAR-10, Figure 18 illustrates our Density-Softmax is one of the best-calibrated models with a low ECE. On the one hand, compared to ERM, MC Dropout, BatchEnsemble, and Deep Ensemble, our model is less under-confidence than them in the prediction that has lower than about 0.4 confidence. On the other hand, compared to ERM, MC Dropout, MFVI BNN, SNGP, and BatchEnsemble, our model is less over-confident than them in the prediction that has higher than about 0.4 confidence. *As a result, accompanying Rank-1 BNN and Deep Ensembles, our*

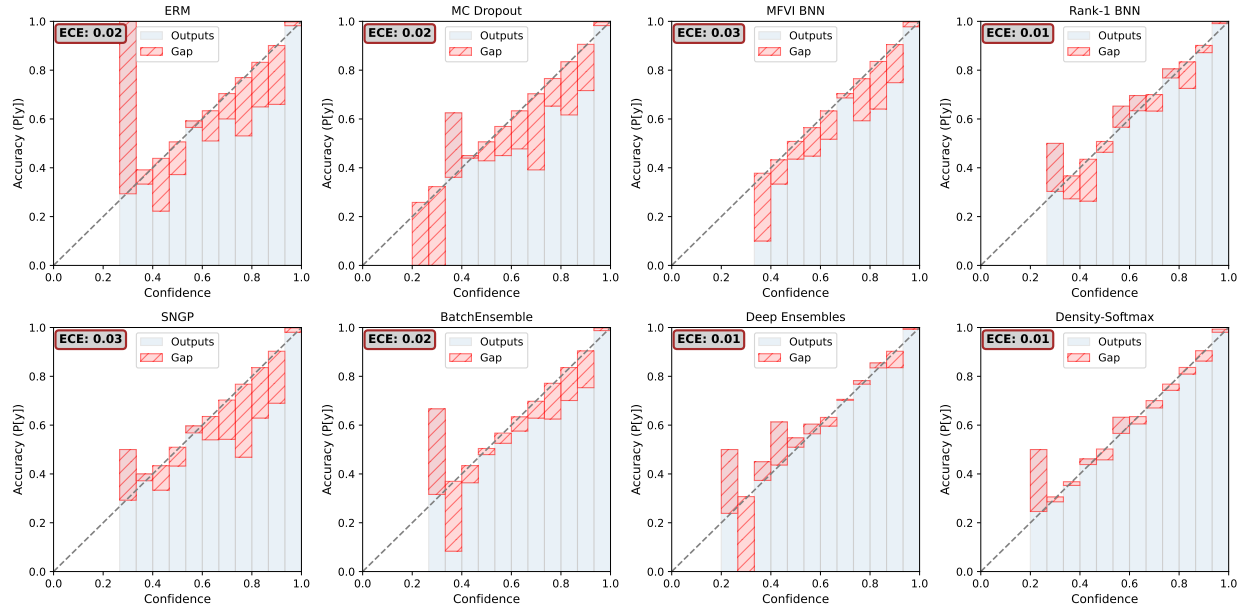


Figure 18: Reliability diagram of Density-Softmax versus different approaches, trained on CIFAR-10, test on IID CIFAR-10. **Density-Softmax has a competitive calibration result with SOTA methods.**

model achieves the best calibration performance on IID data.

More importantly, we find that Density-Softmax is calibrated better than other methods on OOD data in Figure 19 and Figure 20. In particular, Figure 19 shows our model and Deep Ensembles achieves the lowest ECE and less over-confident than others in a particular CIFAR-10-C test set. *Similarly, in real-world distributional shifts CIFAR-10.1 (v6), our model even achieves the lowest ECE with 0.01, outperforms the SOTA Deep Ensembles. These results once again confirm the hypothesis that our model is one of the best reliable models and especially robust under distributional shifts.*

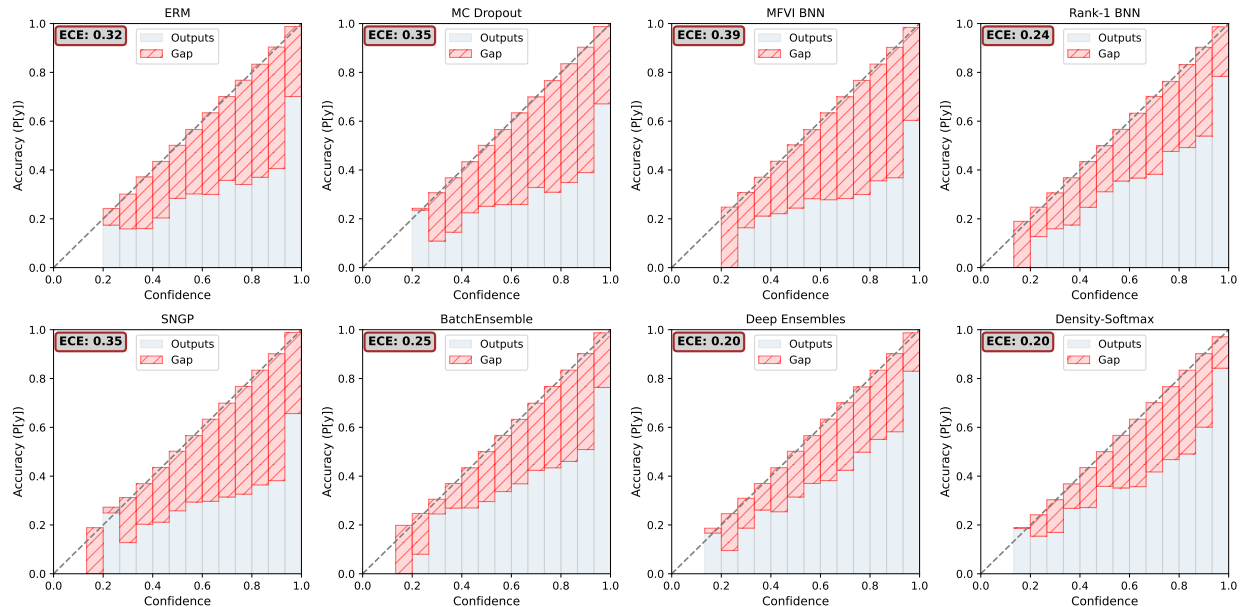


Figure 19: Reliability diagram of Density-Softmax versus different approaches, trained on CIFAR-10, test on OOD CIFAR-10-C set with "frosted glass blur" skew and "3" intensity. **Density-Softmax has a competitive calibration result with SOTA methods.**

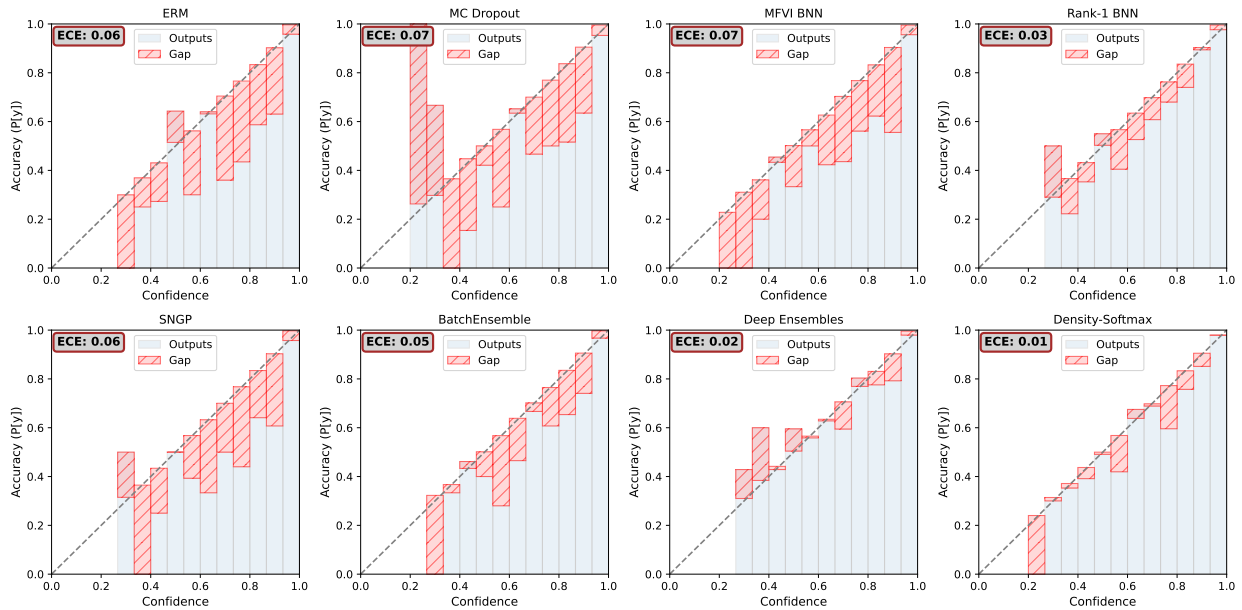


Figure 20: Reliability diagram of Density-Softmax versus different approaches, trained on CIFAR-10, test on real-world shifted OOD CIFAR-10.1 (v6). **Density-Softmax is better-calibrated than other methods.**

Miss-classified Expected Calibration Error. To evaluate the calibration quality in more detail, we continue to make a comparison in terms of Miss-classified Expected Calibration Error [83] as follows

$$\text{mECE}(h) := \sum_{m=1}^M \frac{|B_m|}{N_m} |\text{acc}(B_m) - \text{conf}(B_m)|, \quad (62)$$

where N_m is number of miss-classified samples. This measurement is a specific case of ECE in Equation 2 in the main paper. It is different by covering only the miss-classified samples which are predicted from the forecast $h : \mathcal{X} \rightarrow \Delta_y$. In this case, the lower mECE, the more honest of showing uncertainty if the model actually makes wrong predictions. Figure 21 illustrates the box plots of mECE across shift intensities. *It confirms Density-Softmax achieves the best performance with the lowest mECE, showing the ability to say "I don't know" before it makes the wrong predictions.*

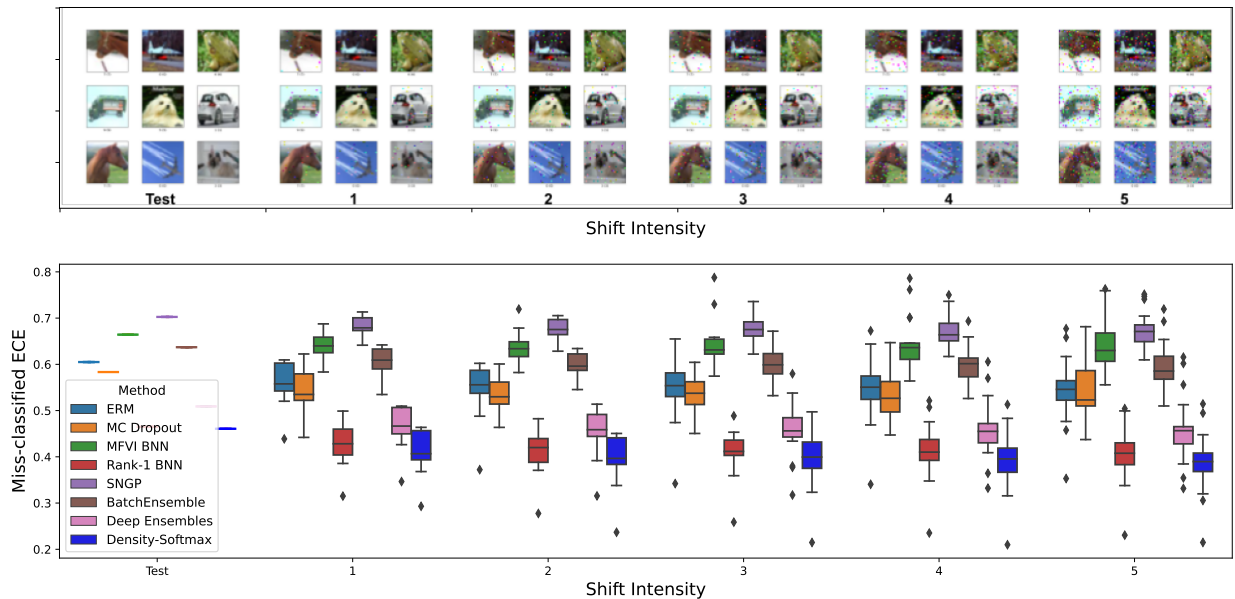


Figure 21: A corruption example by shift intensities and comparison under the distributional shift of miss-classified ECE under all types of corruptions in CIFAR-100-C (setting is similar to Figure 15). **Our Density-Softmax achieves the lowest miss-classified ECE with low variance across different shift intensities.**

C.4.4 Predictive entropy details

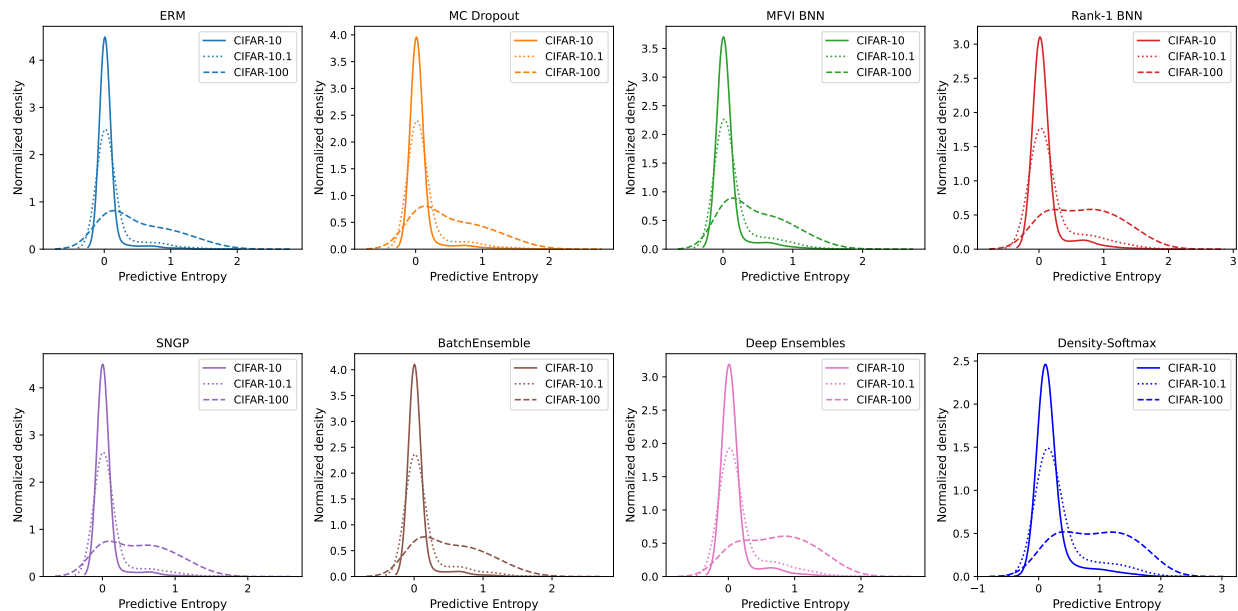


Figure 22: Histogram (bandwidth = 0.5) with density plot details from Figure 3 of predictive entropy for each method on IID testing data CIFAR-10 (solid lines), covariate shift with OOD CIFAR-10.1 (v6) (dotted lines), and semantic shift with completely different OOD CIFAR-100 (dashed lines). **Our Density-Softmax has a low predictive entropy value on IID while achieves the highest entropy value on OOD data.**

Recall that in Figure 3, we have shown our trained model achieves the highest entropy value with a high density. Since this is the semantic shift, the highest entropy value indicates that our model is one of the best OOD detection models. Yet, this is only the necessary condition for a distance-aware model because a pessimistic model could also achieve this performance. Therefore, to prove that Density-Softmax is not always under-confidence, we plot Figure 22. This figure compares density histograms of each method which is trained on CIFAR-10 and tested on IID CIFAR-10, covariate shifted OOD CIFAR-10.1 (v6), and semantic shifted OOD CIFAR-100. We observe that our Density-Softmax has a low predictive entropy with a high density on IID testing data, proving that our model is not under-confidence on IID data. *Combined with the under-confidence on OOD data results, these show our Density-Softmax is a reliability model in terms of distance-aware uncertainty.*